physica status solidi a
www.pss-a.com

Check for updates

Advances in the Use of Atomic Force Microscopy as a Diagnostic Tool for Solar Cells Characterization: From Material Design to Device Applications

Chinedu Christian Ahia and Edson L. Meyer*

Considerable efforts in search for an effective characterization technique for photovoltaic devices with utmost precision is on the increase. For precise analysis and tailoring of device performance, a reliable technique is vital. Atomic force microscopy is one of the leading surface analysis techniques of choice for probing surface patterns in a variety of materials with atomic precision using a cantilever. It has evolved as a reliable technique for the investigation of subatomic scale properties of materials such as photocurrent heterogeneity, electromechanical response, charge distribution, molecular weight effects, and many other material parameters. The integration of artificial intelligence hybrid algorithms in atomic force microscope for optoelectronic device fabrication and characterization has increasingly emerged to be desirable due to its reliability and effectiveness in achieving high image resolution, automated analysis, actuation, and the coupling of manufactured units with a precision down to atomic units. In this review, an investigation of topical developments in the use of atomic force microscopy as a diagnostic tool for solar cells characterization is presented with special focus on polymer solar cells, perovskite solar cells, quantum dots-sensitized solar cells, dye-sensitized solar cells, fullerene-based solar cells, III-V-based solar cells, and silicon-based solar cells.

1. Introduction

There has been concentrated focus on photovoltaic-related research and commitment toward transition from conventional energy resources and their associated negative environmental impact to sustainable energy solutions. Although this is acclaimed as a progressive move, a lot is yet to be done in an effort to develop an innovative technology and sustainable materials with light-harvesting properties that can utilize sunlight efficiently for effective off-grid electricity generation without polluting the environment. Atomic force microscopy (AFM) has progressively become an essential diagnostic instrument of choice for material characterization by reason of modern advancement in probe designs, scan speed, imaging modes, and image resolution (resolved to atomic dimensions). It is renowned as a microscopic technique for the investigation and analysis of diverse materials due to its versatility specifically in offering 3D image visualization and processing of a sample's surface defined to nanoscale dimensions. AFM has evolved tremendously over the years and hence, offers the flexibility of acquiring both quantitative data and high-resolution imaging from a variety of surfaces ranging from solid, liquid, and semisolid materials. It is a nondestructive technique with the capability of investigating the electrical, mechanical, and magnetic properties of materials and requires relatively simple or no sample preparation.

AFM has other advanced functionalities which include measurement of thermal conductivity, piezoresponse, Young's modulus, surface potential, and many more. Due to its extensive adaptability, it suffices to say that AFM is one of the competing cutting-edge imaging and analytical tools for various applications in areas such as in medicine,[1,2] pharmaceuticals,[3] biological sciences,[4] formulation engineering[5] and polymer science.[6] Apart from the aforementioned applications, one of the most intriguing and emerging processes which is currently being applied in the AFM technique is the integration of numerous machine learning (ML) algorithms into AFM for optimum precision during scanning and improvement of image quality. For instance, an automated mechanism for tip functionalization for carbon monoxide molecules which incorporates ML descriptors with computerized software control of the tip has been established.[7] This automated procedure is very crucial for AFM imaging of molecules on surfaces, since the tip functionalization is an essential and laborious process required for submolecular resolution imaging.

The present study highlights key contributions of AFM in solar cell characterization. It also explores emerging opportunities emanating from the use of AFM techniques as a characterization tool. An evaluation of topical developments in the application of AFM and its associated techniques as a diagnostic tool for solar cell characterization with emphasis on polymer solar cells, perovskite solar cells, quantum dots sensitized solar cells (QDSSCs), dye-sensitized solar cells (DSSCs),

C. C. Ahia, E. L. Meyer
Institute of Technology
University of Fort Hare
Private Bag X1314, Alice 5700, South Africa
E-mail: achinedu@ufh.ac.za

The ORCID identification number(s) for the author(s) of this article can be found under https://doi.org/10.1002/pssa.202300293.

DOI: 10.1002/pssa.202300293

 © 2023 Wiley-VCH GmbH

fullerene-based solar cells, III-V-based solar cells, and silicon based solar cells is reported in this work. The results contained in this study proffers a platform toward instituting sustainable solutions to real intricate industrial challenges in the renewable energy sphere.

This work contains five sections which are structured as follows; the article starts with an introductory section. Most of the AFM functionalities which were highlighted in the introduction clearly indicate that AFM has transcended beyond a mere surface analytical technique. The second section contains an overview of AFM operational techniques where the different AFM modes and associated techniques are described. The third section is on material design where a summarized review of the role of AFM and its associated techniques in characterizing different types of solar cells are outlined. The types of solar cells focused on this section are limited to polymer solar cells, perovskite solar cells, QDSSCs, DSSCs, fullerene-based solar cells, III–V-based solar cells, and silicon based solar cells. An overview of some emerging opportunities and applications offered by AFM which has continued to evolve are presented in Section 4, while the present work is concluded with a summary and outlook section.

2. Overview of Atomic Force Microscopy Operational Techniques

AFM is an analytical technique which is primarily based on the measurement of the interactive force between the sample surface and the probing tip situated on a cantilever. **Figure 1** shows a schematic illustration of the fundamental working principles of the AFM system. The to-and-fro motion of the probing tip on the surface of the material is precise to an atomic scale and is regulated by voltages supplied to the X and Y electrodes through the piezoelectric tube, which deflects the tube in a horizontal manner. The photodiodes generate sinusoidal electric signals upon detecting the reflected laser beam from the deflection of the cantilever which is converted into image. Factors such as magnetic forces, chemical bonding, mechanical contact, electrostatic, and Van der Waals forces are mainly responsible for the deflection of the cantilever, while the vertical height of the cantilever is regulated by the application of voltage to the Z electrodes on the piezotube and the length of cantilever deflection calculated through the laser beam reflection from the top of the cantilever. Other cantilever deflection detection techniques apart from the laser beam deflection scheme[8,9] and capacitance sensor techniques[10] include the piezoresistive cantilever detection,[11] tunneling current measurement,[12,13] piezoelectric cantilever detection,[14] and optical interferometer detection.[15]

Basically, there are three fundamental operational modes of AFM which include the contact mode (CM), noncontact mode (NCM), and tapping mode (TM). The development of new types of materials with different structures, dimensions, and the need to investigate their device applications gave rise to other AFM techniques such as the conductive atomic force microscopy (C-AFM)[16] and photoconductive atomic force microscopy (PC-AFM),[17] electrostatic force microscopy (EFM),[18] and Kelvin probe force microscopy (KPFM).[19]

The CM is the most fundamental AFM imaging technique which is more suitable for imaging hard samples that are strongly bonded to the surface. It's a quasistatic mode whereby the tip of the cantilever with spring constant which is preferably less than 1 N M^{-1} is in direct perpetual contact with the surface of the sample during scanning. For CM measurements, the deflection of the cantilever is kept constant using a feedback circuit. This simultaneously ensures that the distance between the tip and the sample surface is kept constant by maintaining a specified force while the topographical image (with nanometer resolution) of the sample surface is extracted by measuring the changes in height of the cantilever deflection. The lateral deflection of the cantilever during CM can be useful in measuring crucial parameters such as the frictional properties of a material.[20] Similarly, the CM is appropriate for recording important

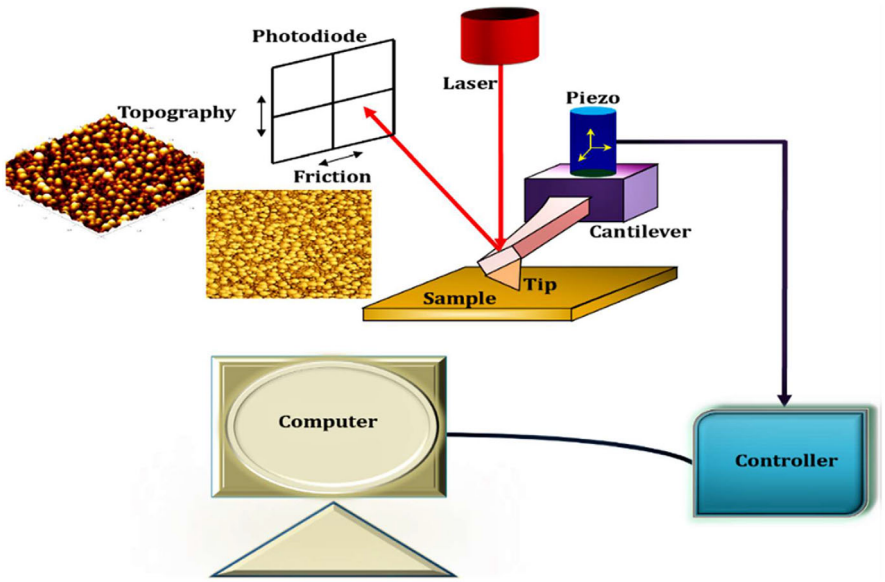

Figure 1. Schematic image describing the operational mechanism of AFM.

© 2023 Wiley-VCH GmbH

18626319, 2024, 3, Downloaded from https://onlinelibrary.wiley.com/doi/10.1002/pssa.202300293 by University Of Fort Hare, Wiley Online Library on [02/09/2025]. See the Terms and Conditions (https://onlinelibrary.wiley.com/terms-and-conditions) on Wiley Online Library for rules of use; OA articles are governed by the applicable Creative Commons License

information regarding the electrical properties of a sample which can be displayed in the form of a 2D image.[21] However, as a result of the force applied to surface friction, the CM is susceptible to surface deformation and displacement of molecules/atoms which can lead to surface reconstruction of the sample surface during scanning. Other challenges of the CM include the rapid wear of cantilever tip which gives rise to erroneous reading. These limitations resulted in the introduction of the NCM and TM-AFM.

In NCM (also known as the frequency-modulation AFM),[22] the probing tip which is influenced by the interaction forces vibrates at a prescribed amplitude and does not touch the surface of the sample during operation. The frequency modulation/NCM is unique for rendering an effective measure of trivial variation in resonant frequency detected by the cantilever due to the enhanced sensitivity of dynamic force microscopy in vacuum offered by this technique. It presents numerous advantages compared with the TM-AFM and can be applied both in air and in liquid. The NCM is more suitable for imaging soft samples such as organic and biological materials due to the long-range interaction between the tip and the sample surface which induces a phase shift between the oscillatory and driving frequencies. The images are obtained in NCM as a result of the change in the frequency of the oscillating cantilever with the amplitude or phase as a feedback parameter.

The TM (also called the "semicontact mode", "intermittent CM", or "amplitude modulation AFM") can be best described as an intermediate state and a hybrid mode between the CM and NCM AFM and was specifically introduced in 1993[23] with the aim of rectifying the inherent limitations and challenges linked with the aforementioned (CM and NCM) conventional AFM imaging techniques. In TM, the probing tip vibrates at a fixed frequency, making periodic contact with the sample surface and disengaging from the surface at intermittent frequencies.[5] The TM AFM is appropriate for imaging samples whose molecules/atoms are loosely bound to the surface on which they are deposited without the danger of displacing or removing the molecules as in the case of contact AFM. Moreover, the TM AFM is associated with increased lateral resolution as a result of the absence of the lateral frictional forces and the coupled stick-and-slip motion of the probing tip existing in the CM AFM.[24] Moreover, an important variant of the TM-AFM imaging is the phase imaging. The phase mode is a technique of sensing and imaging the amplitude and phase change of the cantilever deflection. Using phase imaging technique, vital information in addition to surface shapes can be acquired from phase images. High sensitivity and stability of the feedback is essential so as to observe modifications in amplitude and in the phase of cantilever oscillation in NCM. The amplitude and the phase of cantilever deflections is relative to the interplay between the tip and the surface in the lowest section of cantilever oscillations,[25] while the phase shift corresponds to the force gradient which produces the phase contrast AFM image. The variation of the cantilever oscillation phase is also logged as "phase contrast image".

Apart from the frequency and amplitude modulation techniques in AFM, we also have the force modulation which is similar to the CM AFM. The force modulation is a method to determine the association between the tip and the surface which are regulated by inherent frictional and elastic restoring forces and likewise by intrinsic adhesion existing amongst the tip and the surface investigated. In force modulation, the principles and scanning techniques of the contact mode are employed in observing modifications in sample topography, when concurrently delivering a high-frequency signal to the cantilever. This technique is suitable for materials such as metal alloys and polymer blends and appropriate for measuring alterations in sample adhesion and stiffness. Furthermore, the force modulation microscopy can be used to investigate various nanomechanical properties which rely on the amplitude and phase shift of the cantilever modulation. The C-AFM is a special mode in AFM which is often used in measuring both the topography and the local electrical properties of a material at the point of contact between the tip and the surface of the material. In addition to offering high-resolution topography profiling, C-AFM is an effective current probing technique.[26–30] It is precisely utilized in conducting failure analysis of semiconductor devices and is explored in measuring the local conductivity variations of a sample at nanoscale through the application of DC bias. The C-AFM is mostly operated in either contact or semicontact mode and was first developed in 1993.[16] We also have the PC-AFM mode which is one of the unique AFM variations designed for measuring the photoconductivity and current mapping of a sample surface. Apart from its usefulness in characterizing the electrical properties of materials, PC-AFM is a powerful characterization technique for analyzing solar cell devices and materials, most specifically organic solar cells. It produces high-resolution images using an inverted optical microscope objective as the light source and a neutral density filter. The overall application of PC-AFM in characterizing organic solar cells is niche and information which can be extracted using this technique includes establishing quantum efficiency and power conversion efficiency (PCE) of a device, mapping photoactive regions, measuring concentration of charge carriers and changes in the photocurrent of a material, film morphology analysis, resolving current density–voltage plots, and determination of donor-acceptor domains in a junction. It is also useful in identifying features below the surface of the material down to the nanoscale level. The application of AFM and neural networks has been reported to play a fundamental role in optimizing the fabrication process of organic solar cells.[31] Furthermore, the EFM can be described as an electrical or non-CM of the AFM useful in identifying the dissimilarities in the electric field gradients, charge distribution, and surface potentials of a sample's surface at nanoscale. It therefore provides a platform for comparison and linking the electrical properties of different materials. The presence of electrostatic forces on the surface of the sample triggers a variation in the phase and amplitude of oscillation, which yields information on the electrical properties and charge distribution of the material.

The KPFM is another variant of the AFM which is usually operated in non-CM. It is used in analyzing and generating 3D images of the surface potential of nanostructures at high resolution. Other capabilities of KPFM include topographic analysis and measuring the local work function on a variety of materials at atomic scales. An additional variant of the AFM which is operated in CM by placing the sample (usually a piezoelectric material) surface in proximity with a conductive probe and applying an alternating current (AC) electric field is the piezoresponse

© 2023 Wiley-VCH GmbH

18626319, 2024, 3, Downloaded from https://onlinelibrary.wiley.com/doi/10.1002/pssa.202300293 by University Of Fort Hare, Wiley Online Library on [02/09/2025]. See the Terms and Conditions (https://onlinelibrary.wiley.com/terms-and-conditions) on Wiley Online Library for rules of use; OA articles are governed by the applicable Creative Commons License

force microscopy (PFM). The periodical deformation of piezoelectric samples during scanning enables the PFM to be used in probing the electromechanical properties of the materials such as their nanoscale topography and ferroelectric properties.

The images in **Figure 2** are the contact potential difference (CPD) profiles logged for an electrically open solar cell with the illumination in the range 0–97 mW cm^{-2}. Each potential profile in Figure 2 was determined by averaging the five successive scan lines at sites indicated by the gray line in Figure 5A. The measurement was obtained under the following KPFM conditions: cantilever frequency = 73.74 kHz, cantilever modulation voltage = 560 mV, and lift mode height = 5 nm. A substantial drop in CPD signal is detected over the Ga(In)As junction. The distortions of the profiles recorded at the distance of 3–5 μm are associated with the roughness of the topography.[32] The fundamental operation of KPFM is the lift mode and hence involves numerous drawbacks during image acquisition. Also, as a result of the predetermined tip size of a conventional AFM tip, the CPD is an arithmetic mean of a specified area beneath the tip, which is often greater than the area measured in the topography. This is attributable to the fact that the topographical measurement depends primarily on the gradient of the van der Waals forces which has a shorter range than the electrostatic forces.[33] Lifting the tip away from the surface removes crosstalk between topography and surface measurements, an action which inversely reduces the lateral resolution with increasing tip–sample separation. Moreover, the coupling of topographic measurements and electrostatic information in KPFM can severely affect the topographic measurements. Similarly, the involvement of the whole cantilever toward measuring the electrostatic force can minimize the sensitivity of measurement to a great extent.[34]

For KPFM investigations, several techniques have been proposed by different groups for deconvoluting the topographic measurement from electrostatic information. Some of the proposed approaches include appropriate approximation through analytical calculations,[35] finite-element methods, and numerical simulations.[36–38] Nevertheless, an off-resonant KPFM frequency has been reported to minimize crosstalk with topography, and in

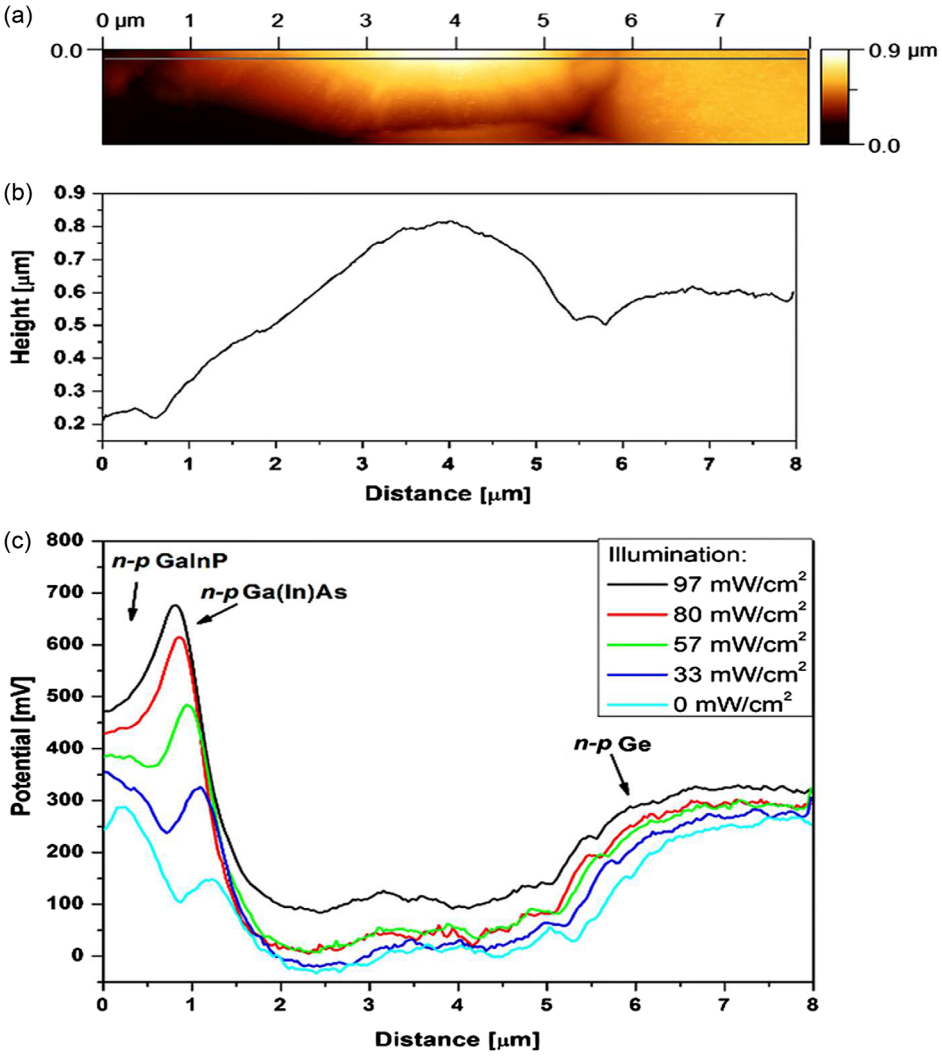

Figure 2. a) Topography image, b) cross section of topography image, and c) KPFM cross-section profiles of an electrically open triple-junction solar cell during illumination under alternating power radiation. Reproduced (Adapted) with permission.[32] Copyright 2014, Elsevier.

© 2023 Wiley-VCH GmbH

18626319, 2024, 3, Downloaded from https://onlinelibrary.wiley.com/doi/10.1002/pssa.202300293 by University Of Fort Hare, Wiley Online Library on [02/09/2025]. See the Terms and Conditions (https://onlinelibrary.wiley.com/terms-and-conditions) on Wiley Online Library for rules of use; OA articles are governed by the applicable Creative Commons License

contrast to lift mode, the topography and surface potential are entirely decoupled given that they are evaluated concurrently.[34] The principal advantage that AM-KPFM offers over lift mode is the propensity to determine the surface potential near the surface, which significantly enhances the lateral resolution of electrostatic forces.

3. Material Design

Over the years, the most renowned material that has been used for solar cells is based on some variation of silicon. Presently, there are several ongoing researches with focus on enhancing the performance of solar cells design. In the same manner, intensified technological advancement specifically in material science due to the quest for improved efficiency, stability, and durability of solar cells at relatively cheap cost of production, a lot of other potential materials are at the moment being explored for potential applications in solar cell devices. Some of such materials include selenide, copper, gallium, etc. can be designed using different components. Solar cell design is a vital procedure for developing extremely efficient solar cells with superior quality and minimal cost. Solar cell design technique includes both material and parameter specification of solar cell structure with the aim of optimizing efficiency, within a specified set of challenges. This section is dedicated toward giving a summarized review of the role of AFM and its associated techniques in characterizing different types of solar cells.

3.1. Polymer Solar Cells

Polymers are materials consisting of periodic chains of molecules. The ability of semiconducting organic polymers to transport charge carriers and excitons is one of the unique properties that enables them to be used in photovoltaic devices. Likewise, they are weightless, adjustable, and are solution processable.[39] Nevertheless, their morphology, crystallinity, phase analysis, and electronic properties can influence the device performance of these materials. AFM can be used to characterize polymeric materials and to investigate polymer crystallization. A feasible approach toward achieving volume morphology and property distribution reconstruction for different types of polymer materials has been described using AFM technique.[40] It is also designed to investigate factors such as crystal melting, sample thickness, reorganizations, and the mechanisms governing the growth of spherulites in polymers. Recently, AFM has been demonstrated as a reliable technique for analyzing complex structural–mechanical surface properties in a wide range of heterogeneous materials such as polymers, polymer composites, and thin films.[41] This was established during a nanoindentation experiment where the subsurface properties of an inhomogeneous synthetic polymer were investigated using AFM at various phases of the tip–surface interaction. Adjustable inelastic modifications of the surface at distinct phases of indentation were confirmed as a function of the nature of both velocity and position of the AFM–tip in the material.[41] An improvement in the ordering and crystallization of polymers due to the addition of solvent additives while preserving the phase-separated morphology in order to enhance the PCE of all-polymer blend solar cells has been investigated using PC-AFM.[42] Results obtained from PC-AFM characterization of the polymer solar cell were beneficial in describing the relationship among the additive-mediated microstructures of the polymer blends including their localized device capabilities.

A conventional conducting polymer known as Poly(3,4-ethylenedioxythiophene)-poly (styrenesulfonate) (PEDOT:PSS) which is renowned due to its transparency, processability, enhanced conductivity, exceptional thermal, and structural stability[43–45] has been characterized using AFM.[46] Information such as the average root-mean-square (RMS) roughness, morphological changes, and surface potential of the polymer was extracted from the investigation. The RMS roughness values of PEDOT:PSS films were observed to increase after the addition of cosolvents, an attribute which is associated with the morphological modification generated in correspondence to the polymer chain. The RMS value of pristine PEDOT:PSS was determined to be 2.6 mm, while the projected average work function of cosolvents-doped PEDOT:PSS thin films is within the range of 4.63–4.82 eV relative to 4.9 eV for the pristine PEDOT:PSS film.[47] Similarly, the homogenous distribution of surface potential of the polymer was deduced with the aid of an AFM line profile. The orientation of polymers within the active layer of an annealed organic polymer solar cell has been reported using a high-resolution AFM phase image.[48] The information obtained from the AFM phase image with regard to the morphology of the organic polymer solar cell can be applied in the control and optimization of the processing parameters during fabrication in order to improve the efficiency of the solar cell.

Additionally, the integration of AFM with infrared spectroscope (AFM-IR) augments the functionality of AFM, hence enabling it as an effective tool for investigating the chemical composition and functional group distribution in polymer films, composites, or blends. AFM-IR can also be employed in conducting thermal measurements through the use of specially designed cantilever probes which can be heated in contact with the samples' surface.[6] Other distinctive capabilities of AFM-IR are that it can be used to provide infrared spectra series in the C–H extended region at different spots on the surface of the sample. Likewise, it can be used for acquiring single spectra and for the production of distribution maps of a signal intensity for a specific wavenumber of choice.[49] AFM-IR has been used to characterize a tertiary blend of conventional commercial polymers including polycarbonate (PC), epoxy resin (ER), and polystyrene (PS)[50] where the results indicate modifications with reference to peak intensities of the C–H bonding in the spectral range of 2920–2970 cm^{-1} as the tip shifted from PC to PS regions. Numerous other applications of AFM-IR spectroscopy in the characterization of polymers have been reported.[51–53] In polymer solar cells, the phase separation and surface morphology of poly(3-hexylthiophene) (P3HT) and [6,6]-phenyl-C61-butyric acid methyl ester (PCBM) blend films have been quantitatively characterized by determining the interface length between the domains of the donor and acceptor using AFM,[54] while the photoactive layer of the polymer has P3HT as a donor and PCBM as an acceptor. The interfacial area of two phases was found to correspond to the short-circuit current density (J_{SC}) of bulk heterojunction (BHJ) solar cells, while its effect on the open-circuit voltage (V_{OC}) is trivial. This shows that an increased interfacial

© 2023 Wiley-VCH GmbH

18626319, 2024, 3, Downloaded from https://onlinelibrary.wiley.com/doi/10.1002/pssa.202300293 by University Of Fort Hare, Wiley Online Library on [02/09/2025]. See the Terms and Conditions (https://onlinelibrary.wiley.com/terms-and-conditions) on Wiley Online Library for rules of use; OA articles are governed by the applicable Creative Commons License

area of donor and acceptor phases is advantageous to the exciton dissociation and carrier transport giving rise to a substantial improvement of J_{SC} and PCE.

3.2. Perovskite Solar Cells

Perovskite-based solar cells have attracted a lot of attention from researchers in recent times due to their cost-effective solution-processing technique (e.g., spin coating), promising PCE (over 22% comparable to competing technologies), and hence are considered as potential alternatives to silicon-based solar cells. Intensified efforts through the use of various deposition and characterization techniques have been reported in numerous studies to explore these categories of materials with the aim of improving their stability. Perovskite thin films are mainly composed of grain microstructures and the size of these grains is responsible for determining the photovoltaic response of the device and their mode of crystallinity. To advance the development and improve the inherent properties of perovskites, the quantitative 3D micrograph of the surface metrics, uniformity, and microstructure of perovskite films can be characterized using AFM. A large extent of perovskites has been reported to be characterized using C-AFM[55–62] and KPFM.[57,63–66] Analysis of results which were extracted from microscopic investigation during the characterization of planar perovskite solar cells reveals favorable influence of grain boundaries which can be attributed to the effective photogenerated charge carrier separation and collection at these boundaries. The application of KPFM toward the investigation of surface defects and band bending near the surface of perovskite thin films which were developed for heterojunction solar cells application gave rise to lower magnitude of surface photovoltage (SPV) signal.[67] The low SPV signal was attributed to the addition of hypophosphorous acid which reduces the density of acceptor-type trap states at the surface,[67] while the rate of SPV is connected to the surface states population which generates band bending.[68] Moreover, the CPD at grain boundaries in perovskite films are susceptible to environmental conditions and was reported to become reduced in the fresh films when exposed to high humidity.[69] This indicates that the nonperovskite phase has its origin from grain boundaries toward grain interiors. In perovskite solar cells, grain boundaries are shown to be a significant contributor to ion migration.[70] Data acquired from measurements of surface potentials and photocurrent of organometal halide perovskite solar cells using KPFM and C-AFM respectively have been reported.[71] These measurements were performed during the scanning probe microscopy (SPM) study of the impact of solvent annealing on the local optoelectronic attributes of perovskite solar devices. The results which were achieved did not only contribute to the atomic-scale knowledge of charge separation in perovskites, but also offered extensive insight on the control process of solvent annealing for device optimization and suggest great effect on the local charge generation and transportation after annealing.[71] Similarly in an attempt to investigate the source of efficiency enhancement in hybrid perovskites, a linear dependence between the grain size and photocurrent has been established using C-AFM in a study which involves the comparison of topography and photocurrent maps.[72] The procedure adopted in the study furnishes a proficient measure for estimating and computing a crystalline quality, so as to achieve a high photovoltaic efficiency. To gain explicit comprehension on the microstructure-confined photovoltaic processes which are responsible for controlling the microstructure of perovskite films in solar cells, several methods which apply the KPFM[73,74] and C-AFM[75] have been implemented in obtaining images which quantify parameters such as the V_{OC}, J_{SC}, PCE, and fill factor with the microstructure of perovskite layer. Besides its usefulness in the investigation of parameters which are related to morphology such as waviness, roughness average (Ra), and RMS roughness, AFM has been described as a complex system for investigating factors such as ferroelectricity, hysteresis, work function mapping, photocurrent, and voltage collection in perovskite solar cells.[76] An assessment of the basic operational principle, development mechanism of C-AFM technology, and the modern applications of C-AFM in perovskite solar cells have been thoroughly reviewed.[77] The precise influence of photogenerated carrier/ion transport characteristics within the material and at the surface/interface, together with the established ferroelectricity and polycrystalline orientation, on the device efficiency, stability, and hysteresis, was described in the study.[77]

A special method which relies on tomographic AFM has been implemented in realizing an entirely-3D, photogenerated carrier transport map at the atomic scale in hybrid perovskites. Information obtained using the aforementioned methodology can be vital for augmenting hybrid perovskites for numerous optoelectronic applications such as in solar cells and photodetectors.[78] Likewise, the surface features of a family of fullerene derivatives have been effectively characterized using AFM in order to improve the ambient stability of perovskite solar cells.[79] Generally, among all AFM variants, KPFM is contemplated as an auspicious technique to investigate surface trap states in perovskite materials.[68]

3.3. Quantum Dot Sensitized Solar Cells

Quantum dot (QD)-based solar cells have attracted a surge of interest in view of their promising application as light harvesters.[80] Evaluation of results obtained from computed data has shown that the introduction of multilayers of self-assembled QDs within the intrinsic region of p–*i*–n structure can considerably enhance its conversion efficiency.[81] QDSSCs are classified as third-generation solar cells. In QDSSCs, the QDs act as the sensitizer and photon-absorbing materials. They are promising alternatives for silicon, copper indium gallium selenide (CIGS), or cadmium telluride (CdTe)-based solar cells due to their wide tunable bandgaps and absorption range, simple solution processability, remarkable aptitude for producing multiple excitons, and retarding the cooling process of excited electrons. Significant progress has been achieved in the characterization of QDSSCs using AFM. Some of such advancements include the estimation of the rms roughness and the extrapolation of a suitable roughness value for efficient electrocatalytic reactions in a series of novel composite cobalt–copper sulfide (CoS-CuS) counter electrodes which were developed for application in QDSSCs.[82] In an attempt to enhance the J_{SC} in QDSSCs through the advancement of the deposition of QDs in mesoporous TiO_2 photoanodes

© 2023 Wiley-VCH GmbH

18626319, 2024, 3, Downloaded from https://onlinelibrary.wiley.com/doi/10.1002/pssa.202300293 by University Of Fort Hare, Wiley Online Library on [02/09/2025]. See the Terms and Conditions (https://onlinelibrary.wiley.com/terms-and-conditions) on Wiley Online Library for rules of use; OA articles are governed by the applicable Creative Commons License

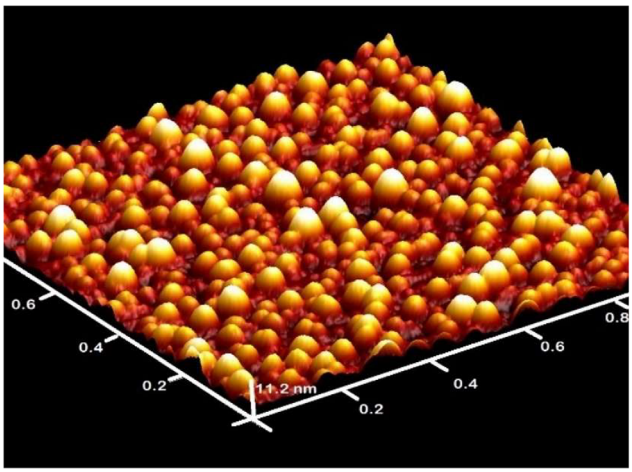

Figure 3. 3D AFM image of uncapped QDs acquired using tapping mode conditions.

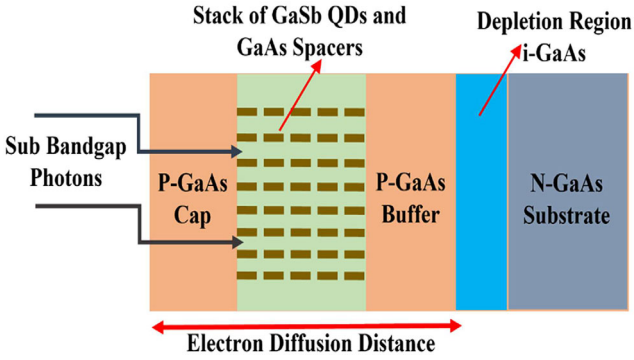

Figure 4. Schematic of quantum dot intermediate band solar cell with the GaSb quantum dots implanted between the GaAs buffer and cap regions which are situated outside the GaAs p–n junction depletion region.

containing SiO_2 nanoparticles by cladding them with ultrathin TiO_2, 3D AFM micrographs obtained from this study propose that the ultrathin-TiO_2 shell in SiO_2/TiO_2 core/shell nanoparticles can be effective in regulating the unfavorable QDs growth result of SiO_2 nanoparticles within the TiO_2 photoanode.[83]

Figure 3 shows the AFM image obtained from a sample containing metal–organic vapor phase epitaxial grown InSb QDs on GaSb substrate. Information such as the surface morphology, quantum dot size distribution, dimensions, and areal density can be extracted from the image analysis for the optimization of growth parameters to achieve improved device efficiency. Detailed description on how the properties of the deposited material can be extracted from the AFM image and the effect of factors such as the V/III ratio, buffer layer, and substrate orientation on materials deposition has been reported elsewhere.[84,85] Furthermore, AFM has been used to comprehensively investigate the effect of Cu doping in CdS QDs during a study involving the fabrication of QDSSCs using successive ionic layer adsorption and reaction (SILAR) technique with the aim of improving the photovoltaic performance.[86] Similarly, the tapping-mode AFM technique has recently been reported to facilitate the surface morphology evaluation of CdS QDs-sensitized FTO/TiO_2 electrodes which were prepared using SILAR method in a comparative investigation on QDSSCs for performance optimization.[87] A lot of other similar studies where AFM played a major role in the characterization of QDSSCs have been reported.[88–92]

Figure 4 depicts a simplified schematic of QD intermediate band solar cells. In an investigation which was focused at formulating stacks of QD with trivial strain for intermediate band solar applications, AFM was applied to facilitate the establishment of improved uniformity in QD size distribution and areal density which was accomplished through vertical ordering of the dots successively with the objective of achieving strain compensation in the dot layers.[93] Correspondingly, AFM has aided the confirmation of good lateral ordering of QD during the deposition and characterization of InGaAs/GaAs QD superlattices for intermediate band solar applications.[94] Other AFM-assisted measurements include the estimation of areal density for intermediate band solar cell.[95–98]

With the exception of topographic high resolution micrographs, spatial properties parallel and perpendicular to the surface as well as localized trends and features in materials such as adhesion and stiffness,[99] current mapping through C-AFM,[100] QD agglomeration,[101,102] and phase homogeneities of CuS counter electrodes at different deposition times[103] have been reported from AFM measurement during the characterization of QDSSCs and have consequently enabled precise extraction of information on the material properties required for the fabrication of high-efficiency QDSSCs. Results emanating from these studies and many others provide a unique knowledge for the development of next-generation solar cells with optimized efficiency.

3.4. Dye-Sensitized Solar Cells

DSSCs are a special class of thin-film solar cells which are categorized as third-generation solar cells like the QDSSCs. They are mostly renowned for their cheap cost of production, potential for high efficiency and their relatively simple fabrication method. They generally consist of a redox electrolyte, a translucent dye-sensitized mesoporous TiO_2 working electrode, and a translucent counter electrode. The morphology of the dye layer can play a vital role in determining the effectiveness and efficiency of a DSSC. An improvement in the amorphicity and roughness value of composite electrolyte thin films which were determined with AFM during the fabrication of solid-state DSSC prompted an enhancement in the photovoltaic performance of DSSC.[104] In another study, AFM played a useful role in investigating the surface parameters and formation process during the fabrication of more permeable composite films of poly(3,4-ethylenedioxythiophene) and functionalized, multiwalled, carbon nanotubes (CNTs) as counter electrodes for DSSC.[105] Furthermore, during the development of CdS on TiO_2 surface using various chemical deposition procedures and the study of their various effects on the performance of DSSC, AFM was used to establish the influence of each deposition technique on the porosity and surface morphology of the electrode which ultimately alters their optical properties and affects the efficiency of the DSSC.[106] AFM has enabled the surface morphological evaluation and characterization of different types of films in several studies[107–112] for

© 2023 Wiley-VCH GmbH

18626319, 2024, 3, Downloaded from https://onlinelibrary.wiley.com/doi/10.1002/pssa.202300293 by University Of Fort Hare, Wiley Online Library on [02/09/2025]. See the Terms and Conditions (https://onlinelibrary.wiley.com/terms-and-conditions) on Wiley Online Library for rules of use; OA articles are governed by the applicable Creative Commons License

DSSC application. Some of these thin films include neodymium oxide and erbium oxide-doped titania films,[113] nickel nitride film,[114] graphene film,[115] reduced graphene oxide film,[116] TiO_2 film,[117] poly(dimethyldiallylammonium chloride) on TiO_2 and poly(sodium 4-styrenesulfonate) on TiO_2 nanocomposite films,[118] undoped NiO, and Li doped NiO thin films[119] among many others. The application of AFM technique was fundamental in confirming the surface features of ZnO compact layers which was infused into a photoelectrode at the interface between nanocrystalline ZnO/FTO layers in an attempt to enhance the efficiency of a ZnO DSSC.[120] AFM was instrumental in monitoring the course of dye adsorption in situ with the purpose of estimating the thickness and homogeneity of N719 dye adsorption on titania for DSSC applications.[121] Additionally, the evaluation of surface complexity and fractality of highly ordered TiO_2 nanotubes using AFM has been investigated for photoelectrode application in DSSC.[122] The increased number of surface morphology investigations on different thin films for DSSC applications has validated AFM as a method of choice for determining the structural and optical properties desired for an efficient absorber material in DSSCs.

3.5. Fullerene-Based Solar Cells

Fullerenes are chains of hollow carbon molecules. It is an allotrope of carbon with its molecule made up of carbon atoms which are fused in such a way as to generate a closed or relatively closed network. Numerous new fullerene-based acceptors have been projected for the purpose of enhancing the efficiency of polymer solar cells on account of their favorable properties.[123] The AFM approach has been used to establish the different domain feature sizes in blended films made from squaraines during the atomic scale characterization of squaraine fullerene-based photovoltaic active layers.[124] During the study,[124] topographical maps which were generated in peak force tapping mode and maps of the surface potential in KPFM mode were developed to explore the nanomorphology of BHJ films indicative of the effective squaraine-based organic photovoltaic (OPV) devices.

AFM has enabled the in-depth understanding of surface features in P3HT:PCBM films which were used both as an active layer during the fabrication of noninverted fullerene-based organic solar cells[125] and in another study which was aimed at confirming the influence of film treatment on the performance of P3HT/soluble fullerene-based organic solar cells.[126] The P3HT:PCBM thin films were supplementarily analyzed with C-AFM to observe both the hole and electron transport mechanism and to further verify the function of the linear polyethylenimine layer.[125] Similarly, the surface morphologies of ultrathin $sMoO_3$ films which can function as an effective anode interfacial layer in polymer/fullerene-based solar cells have been thoroughly evaluated using AFM, with the results indicating that the $sMoO_3$ film spin coated from its aqueous solution could function as an exceptional anode interfacial layer with similar cell efficiency in comparison with PEDOT:PSS, even though the device stability pertaining to $sMoO_3$ was significantly improved.[127] In a study which involves the optimization of solution-processed oligothiophene,[128] AFM analysis of the photoactive layer in a fullerene-based organic solar cell has provided clear comprehension into the distribution of donor and acceptor within a blend containing quinquethiophene DCV5T-Bu_4 as donor in conjunction with $PC_{61}BM$ as acceptor.

Furthermore, the application of time-resolved electrostatic force microscopy (trEFM)[129–131] has been employed in a study to map spatial dissimilarities in external quantum efficiencies occurring from subgap charge transfer excitation in polymer/fullerene-based solar cells.[132] The results indicate that the local distribution of photocurrent caused by the charge transfer states is almost similar to the spatial difference in external quantum efficiencies from above-gap singlet excitation.[132] Further applications of AFM analysis on fullerene-based solar cells include in the surface morphology characterization of the various blend films,[133–136] in the observation of the phase separation morphologies of four different fullerene-based blend films which were developed using optimal conditions,[137] in determining the crystallinity and surface morphologies of BHJ of fullerene-based polymer solar cells,[138] and in the conductivity/photoconductivity and the nanoscale morphological examination of a newly fabricated fullerene-based solar cell system based on tetrabenzoporphryin (BP) and PCBM using C-AFM and PC-AFM.[139]

3.6. III–V-Based Solar Cells

III–V compounds are alloys which comprise group III and V elements as classified from the periodic table. They are characterized by high electron mobility and usually crystallize in zinc blende structure while their nitrides crystallize in the wurtzite crystal structure. Their ability to absorb the light's energy from concentrated sunlight and transmit the absorbed energy to the electrons in the material makes them useful for application in solar cells. Most importantly, III–V compounds form a major part of multijunction concentrator solar cells which have been reported to yield the highest efficiency of 47.1% compared to other photovoltaic technology to date.[140]

The morphological features of SiGeSn[141] and GaInP/GaAs[142] have been evaluated by means of AFM during the fabrication of III–V-based solar cells, while the electrical properties of III–V (GaAs) nanowire-based solar cells have been studied using C-AFM.[143] Nanoscale variations in surface roughness and topography of GaAs-based solar cells were established using AFM during a performance analysis investigation which reveals that a modification in the surface structure ultimately affects the efficiency.[144] Likewise, KPFM technique has been exploited to qualitatively investigate the built-in potential and voltage drops across multijunction III–V solar cells.[32] Results provided from this study[32] can be useful in delivering a response toward revamping the design of photovoltaic devices and present supplementary understandings into behavior of the multijunction solar cell.

Figure 5 contains C-AFM topographic image and current mappings which were obtained while applying a bias between tip and sample. The examined region is constant in all images, which implies that the images are not drift corrected. From Figure 5B–E, the measured current values in the images are depicted in gray color scale with range from −50 to +50 pA. The different colors of circles are used to emphasize the spots of designated NWs in different images. Majority of the NWs do not conduct considerably at roughly 0.5 V of bias, although few vary from the conventional

© 2023 Wiley-VCH GmbH

18626319, 2024, 3, Downloaded from https://onlinelibrary.wiley.com/doi/10.1002/pssa.202300293 by University Of Fort Hare, Wiley Online Library on [02/09/2025]. See the Terms and Conditions (https://onlinelibrary.wiley.com/terms-and-conditions) on Wiley Online Library for rules of use; OA articles are governed by the applicable Creative Commons License

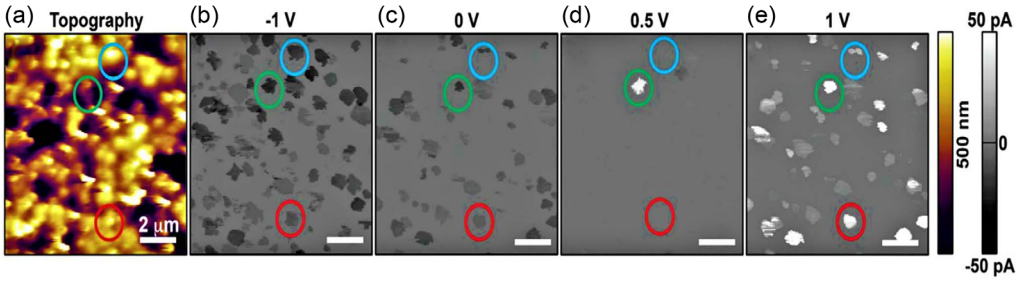

Figure 5. A) C-AFM topography image and B–E) and current maps of GaAs nanowires ensemble acquired from the scanned surface using contact mode while applying different voltages between tip and sample under light illumination. Reproduced (Adapted) with permission.[143] Copyright 2017, Elsevier.

mode such as the blue and green circles in Figure 5D. This mirrors the fundamental inhomogeneity of the electrical properties of the GaAs NWs and confirms the peculiarity of the V_{oc} to each NW,[143] as shown in **Figure 6**.

Furthermore, AFM studies on the crystallinity and surface roughness of a 5 μm-thick Ge epilayer on bulk Si and on a low porous Si buffer layer have shown that low-porosity buffer layer is favorable for the deposition of low-defect-density Ge on Si virtual substrates for the subsequent incorporation of III–V multijunction solar cells on Si.[145] C-AFM has been described as a reliable technique for analyzing structural defects such as the existence of antiphase domains which acts as nonradiative recombination centers during GaAs heteroepitaxial deposition of Ge for photovoltaic applications.[146]

Figure 6 shows the voltage measurements acquired for each of the junctions from the GaAs ensemble displayed in Figure 5. The V_{oc} distribution displayed in Figure 6 ranges from 0.25 to 0.6 V. The estimated consolidated V_{oc} of the NWs coupled in parallel ($<V_{oc}>$) and the V_{oc} of the NW ensemble device (V_{oc}^{dev}) are delineated on the graph by vertical lines. The inset reveals 3 *I–V* curves under the light which are the least effective NW junction (red) and the best performing NW junction (blue) from the deduced statistics including the estimated sum *I–V* of the virtual device (green) with the average current.[143]

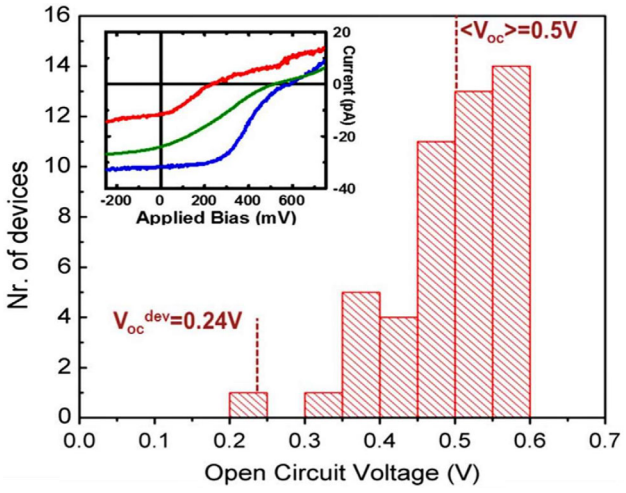

Figure 6. V_{oc} statistics of ensemble of GaAs NWs extracted from C-AFM measurement. Reproduced (Adapted) with permission.[143] Copyright 2017, Elsevier.

AFM has facilitated the investigation of metamorphic structures originating from ideal strain relaxation in GaInP/GaAs/InGaAs inverted metamorphic solar cells to establish lattice matching and photocurrent matching of subcells.[147] Information deduced from numerous other studies reporting the use of AFM for inspecting the surface morphology[148,149] and roughness[150,151] in III–V-based solar cells indicates that it is an essential tool for monitoring process development and quality control of materials.

3.7. Silicon-Based Solar Cells

Silicon is the most common material used in solar cells. Silicon-based solar cells achieve high efficiencies, but their cost of production is relatively expensive and they have relatively limited life cycles. Different AFM modes/techniques such as the C-AFM and KPFM have been used to investigate the cross section of silicon solar cells with the intention of measuring the local electrical properties of the device which include SPV and photocurrent.[152] The implementation of sensitivity-enhanced KPFM technique has facilitated the observation of surface potential in silicon-based solar cells,[153] while the mapping of local electronic transport properties in hydrogenated microcrystalline silicon using AFM which is equipped with a conductive cantilever has been used to investigate the dependence of layer thickness with surface roughness, crystallite size, and conductive region.[154] Measurements using PC-AFM and KPFM have been employed in assessing the photovoltaic effect of poly-silicon-based solar cells and also in monitoring the alterations in surface potential, which come from the accumulated photoinduced carriers on the surface of the device.[155] The influence of surface properties for textured silicon substrates has been explored with AFM for potential light trapping applications in silicon solar cells, with results suggesting that modulated texturing of silicon substrates can be beneficial in the augmentation of photoconversion and the efficiency of silicon solar cells.[156] Most importantly, the first successful mapping of photocarrier lifetimes on silicon nanocrystal-based solar cell structures using KPFM has presented an analytical approach on conducting KPFM lifetime measurement with a higher lateral resolution for surface potential investigation and with satisfactory precision.[157]

The image displayed in **Figure 7** was obtained under tapping mode AFM condition from a degraded solar cell structure containing heterojunction with intrinsic thin layer (HIT). The surface morphology of the degraded solar cell is characterized by

© 2023 Wiley-VCH GmbH

18626319, 2024, 3, Downloaded from https://onlinelibrary.wiley.com/doi/10.1002/pssa.202300293 by University Of Fort Hare, Wiley Online Library on [02/09/2025]. See the Terms and Conditions (https://onlinelibrary.wiley.com/terms-and-conditions) on Wiley Online Library for rules of use; OA articles are governed by the applicable Creative Commons License

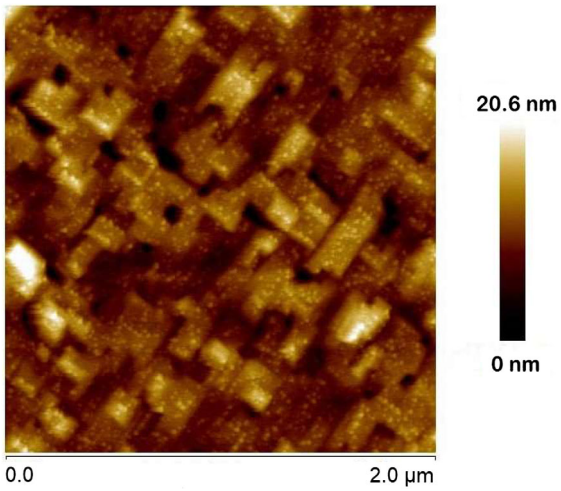

Figure 7. 2D AFM topographic micrograph of degraded photovoltaic cells showing structural defects.

defects as seen in the micrograph and hence, the technique can be useful in addressing long-term solar cell degradation challenges which are linked with defects. Information on the scan parameters and procedure used in acquiring the micrograph in Figure 7 is comparable to what has been reported elsewhere.[158] Similarly, with the assistance of a conducting diamond tip, the presence of the radial p–n junctions for purposefully fragmented silicon nanowire solar cells has been confirmed through the application of a current mapping mode in the conducting AFM.[159] The outcome of the finding is expected to eliminate the economic viability challenges linked with the photovoltaic market. Furthermore, the conductive channel,[160,161] electronic properties,[162,163] and surface roughness[164–166] of silicon solar cells and thin films respectively have been characterized using C-AFM with results which were obtained from experimental observation corresponding to that of numerical calculations.

The summary of material properties for solar cell application that has been characterized using various AFM techniques and reported from carefully chosen data (within the year 1995 and 2021) is shown in **Table 1**. The information displayed in Table 1 is reported for materials specifically applicable in polymer solar cells, perovskite solar cells, QDSSC, DSSCs, fullerene-based solar cells, III-V-based solar cells, and silicon-based solar cells.

4. Applications and Emerging Opportunities

AFM has been an effective imaging technique for studying materials beyond atomic scale since the past 3 decades. It is a versatile tool with various applications in material science, biological sciences, physical sciences, semiconductors and electronics, research institutes, and academics. AFM offers diverse modes for analyzing different material properties, such as the topography, conductivity, surface potentials, capacitance, elasticity, adhesion, friction, electrical properties, and magnetic force. Owing to this, several applications and emerging opportunities for AFM which transcend beyond ultraprecision manufacturing, smart machining, biomedicine, nanotechnology, and many others have continuously attracted the attention of different researchers and manufacturing entities. Interestingly, AFM has been reported by some researchers to sustain the generation of quantum spin states in quantum computing, thereby granting the qubits that could conceivably propel substantially faster computers eventually.[167] It is an enabler toward the control and advancement of clean technologies attributable to its indispensable role in the development of lithium-ion batteries. An overview of some emerging opportunities offered by AFM which has continued to evolve is presented in this section.

4.1. Machine Learning and Artificial Intelligence

By developing an artificial intelligence (AI)-based platform which employs automated tip functionalization via ML in AFM, the influence of cantilever vibration, Van der Waals forces, scan parameters, friction, and their relationship with image quality could be explored and improved on for further advanced applications. Furthermore, the incorporation of ML in AFM technique introduces the opportunity for a distinctive and disruptive withdrawal from the types of both experimental and theoretical procedures which have formed the foundation of the field of SPM following its commencement in the eighties.[12,168] The remarkable progress achieved in ML-assisted probe microscopy during the past years indicates that we are at the frontiers of developing a more innovative approach to the technique: next-generation SPM, where the functional throughput and investigative parameters of probe microscopy are augmented considerably by AI approaches.[169] An outline which illustrates the integration of AFM-based datasets (pc-AFM, KPFM, etc.) and macroscopic *J–V* measurements with the aim of engineering a data feature of reduced dimensions (in comparison to the input data) without modifying the variability of the circumstance to be defined has been described using AI algorithms.[66] Information extracted from the process was utilized in configuring the artificial neural network through the controlled learning stage. Recently, a technique for combining AFM images into a ML model in order to determine the PCE of binary (polymer and Non-Fullerene Acceptor molecule) BHJ-OPVs was reported.[170] The study effectively determined vital spatial wavelengths between a large dataset and displayed an approach toward alternative coherent BHJ OPVs. A high level of skill set, experience, and precision is often required in fine tuning AFM scan parameters in order to acquire a high-resolution AFM image. The complexity involved in obtaining such images at submolecular resolution is time consuming and can be ameliorated through the application of ML and AI in tuning the scan parameters (such as the scan rate, integral gain, drive amplitude, and setpoint) to optimal values during real-time image acquisition when capturing AFM measurements. The integration of ML and AL algorithms into AFM can also be useful as an indispensable technique for differentiating underlying materials from nanoparticles and hence for the precise analysis of images obtained from AFM measurements through particle identification.

4.2. Micromachining

Micromachining is a pioneering manufacturing process which is predominantly used by scientists, engineers, and biomechanics

© 2023 Wiley-VCH GmbH

18626319, 2024, 3, Downloaded from https://onlinelibrary.wiley.com/doi/10.1002/pssa.202300293 by University Of Fort Hare, Wiley Online Library on [02/09/2025]. See the Terms and Conditions (https://onlinelibrary.wiley.com/terms-and-conditions) on Wiley Online Library for rules of use; OA articles are governed by the applicable Creative Commons License

Table 1. Selected data on materials characterization using AFM techniques for solar cell application.

Type of material (Design)	Technique used	Property investigated	Year reported	References
Polymers	AFM	Subsurface structure	2021	[41]
		Phase separation	2015	[54]
		RMS roughness, Morphological changes	2019, 2017, 2010	[47,48,196]
	KPFM	Surface potential, SPV	2023	[197]
	PC-AFM	Surface topography, Current images	2022	[42]
Perovskites	C-AFM, KPFM	Photocurrent, Surface potential, Charge separation and collection at the grain boundaries, Topography, Microstructure	2015, 2016, 2017, 2018, 2019	[55–65,71–75]
	KPFM	Work function, Hysteresis [current density–voltage (J–V) curve)]	2019	[76]
	C-AFM	Current mapping, I–V Hysteresis	2023	[198]
	KPFM	Surface trap, Surface potential	2023	[198]
	KPFM	Degradation processes	2018	[69]
	PFM	Ferroelectricity	2019, 2021, 2023	[76,199,200]
Quantum dots	AFM	Surface features through high resolution micrographs	2015, 2016, 2017, 2020, 2021	[87–92]
		QD size distribution and areal density	2006, 2012, 2014	[93,95–98]
		Lateral ordering	2005	[94]
		QD agglomeration	2009, 2015	[101,102]
		Phase homogeneities	2015	[103]
		Surface morphology & Cross section	2023	[201]
		Adhesion and stiffness	2019	[99]
	C-AFM	Current mapping	2019	[100]
Dye/Thin film layers	AFM	Surface morphology and roughness	2003, 2007, 2008, 2010, 2011, 2012, 2013, 2014, 2015, 2018, 2019, 2023	[104–120,122,202]
		Thickness and homogeneity	2010	[121]
Squaraine-fullerene	KPFM	Domain feature sizes and topographical maps	2019	[124]
P3HT:PCBM films for fullerene-based solar cells	C-AFM	Surface complexities and features, Hole and electron transport mechanism	2008, 2016	[125,126]
Various blend films for fullerene-based solar cells	AFM, C-AFM	Crystallinity, Surface morphologies, Phase separation	2010, 2013, 2016, 2019, 2020, 2021	[127,133–136,138]
Polymer/fullerene-based solar cells	trEFM	Mapping spatial dissimilarities, and local distribution of photocurrent	2015	[132]
Solution-processed oligothiophene (photoactive layer in a fullerene-based organic solar cell)	AFM	Mapping distribution of donor and acceptor	2013	[128]
Tetrabenzoporphryin (BP) and PCBM.	C-AFM, PC-AFM, AFM	Photoconductivity, Nanoscale morphology	2011	[139]
Semiconductors and III-V compounds	AFM	Morphological features, Crystallinity, Surface roughness	2010, 2014, 2015, 2018, 2020, 2021	[141,142,144,145,148–151]
	C-AFM	Electrical properties, structural defects (existence of antiphase domains)	2011, 2017	[143,146]
	AFM, C-AFM	Surface Morphology, Lattice matching and photocurrent matching of sub cells	2019	[147]
	KPFM	Built-in potential and voltage drops	2014	[32]

© 2023 Wiley-VCH GmbH

18626319, 2024, 3, Downloaded from https://onlinelibrary.wiley.com/doi/10.1002/pssa.202300293 by University Of Fort Hare, Wiley Online Library on [02/09/2025]. See the Terms and Conditions (https://onlinelibrary.wiley.com/terms-and-conditions) on Wiley Online Library for rules of use; OA articles are governed by the applicable Creative Commons License

Table 1. Continued.

Type of material (Design)	Technique used	Property investigated	Year reported	References
Silicon solar cells	C-AFM, KPFM	SPV and photocurrent	2016	[152]
	PC-AFM, KPFM	Surface potential, photovoltaic effect	1995, 2013	[153,155]
	AFM, C-AFM	Local electronic transport properties, layer thickness, surface roughness, crystallite size, the presence of the radial *p*-n junctions and conductive region	1999, 2000, 2001, 2002, 2009, 2010, 2011	[154,159–166]
	AFM	Surface/Morphological properties	2018, 2023	[156,203]
	KPFM	Photo-carrier lifetime	2014	[157]

in industrial research and development to reconstruct systems at a microscopic scale through the application of geometrically defined cutting edges. It is a powerful technique for altering the surface properties/integrity of a material to desired microstructures. During this procedure, the scanned AFM probe is fundamentally employed in situ to systematically planarize a sample site selectively, thereby gradually exposing the concealed microstructural features of interest. Micromachining can be very useful for acquiring multiple numbers of high-fidelity photocurrent maps over a range of polished depths hence, creating clear insight toward optimizing charge transport in hybrid perovskite thin films for device applications such as in solar cells.[78] Studies involving the use of AFM diamond tip and precision stage to execute micromachining have been reported during which machining parameters such as the amount of feed, velocity, and applied force were investigated to establish their influence on the process of micromachining.[171] Likewise, by optimizing the control algorithm and adjustment coefficients, an effective technique to machining which is based on 3D microstructures has been utilized in the micromachining system to resolve the challenges which are associated with AFM during the machining process.[172] The AFM tips/probes which are often designed using silicon can be modified via micromachining approach to achieve ultrahigh sharpness, increased sensitivity, favorable density, and resonant frequency which are critical features mandatory for the production of high-quality images. Besides enabling high-resolution unveiled nanofabrication procedures for arbitrary nanodesigns, AFM-based nanomachining is essential in understanding and controlling the machine parameters for fabricating nanopatterns and tailoring the designs to desired dimensions of choice.[173]

4.3. Nanofabrication and Nanomanipulation

These are emerging processing techniques which are capable of realizing high-precision and high-quality adjustment and machining during the development, design, and engineering of nanoscale structures with dimensions down to atomic scale. The fabrication of nanostructures and devices at atomic scale can be achieved using AFM technique, with the AFM probe which consists of the cantilever and the tip as an indispensable component and enabler during the process. Similarly, the application of AFM probe in nanomanipulation is an effective procedure for the arrangement of nanoparticles into intricate configuration through the automatic and precise identification of the nanoparticles on the substrate. Nanofabrication has been used by many researchers for surface deposition and amendment.[174,175] For instance, AFM in contact mode in air has successfully been used for the deposition of nanostructures of silicon on a H-passivated Si(100) substrate by means of mechanical friction.[176] A review of AFM-based nanofabrication methods of silicon using mechanochemical local oxidation and additional significant characterization techniques has been discussed by other authors,[177] while a recommendation for the modification of industrial AFM systems to realize improved cutting speeds for nanoelectromechanical systems and associated semiconductor devices has been outlined.[178] Other AFM tip-based nanofabrication methods include the electrochemical oxidation method,[179] thermal probe lithography,[175] material transfer,[180] and removal technique.[181] Likewise, a deep learning algorithm has been proposed by some researchers recently as an autodetection technique for flexible nanowires in AFM micrographs.[182] Images displaying nanoscale grooves which were obtained from AFM are shown in **Figure 8**, in addition with their corresponding cross sections, for the case where the feed direction was "edge forward".

4.4. Biomedicine

The role of AFM in biomedical research cannot be overemphasized. Significant progress has been made in the use of advanced AFM techniques to characterize living cells and in obtaining high-resolution images (at submolecular level) from biomedical samples. Such advancements are beneficial for the effective visualization and investigation of dynamic biomedical processes. The propensity of AFM to measure electrostatic properties is also among the emerging advances that can assist the investigation of biological and biomedical samples.[183]

For instance, AFM is at the moment being utilized for the investigation of different kinds of bacteria,[184] protein molecules,[185] and viruses[186,187] for monitoring purposes, with a focus on gaining precise knowledge about the actions of complex biological systems. It also plays a vital role in DNA and chromosome investigations, specifically in the structural analysis of chromatin and metaphase chromosomes.[188,189] As a result of the extension of AFM functionalities toward the biomedical field, it has been envisaged that AFM can evolve toward acting as a bridge to the fabrication of personalized medicine.[1] Presently, AFM has been reported as a diagnostic tool for the assembly and mapping of human diseases respectively.[1]

© 2023 Wiley-VCH GmbH

18626319, 2024, 3, Downloaded from https://onlinelibrary.wiley.com/doi/10.1002/pssa.202300293 by University Of Fort Hare, Wiley Online Library on [02/09/2025]. See the Terms and Conditions (https://onlinelibrary.wiley.com/terms-and-conditions) on Wiley Online Library for rules of use; OA articles are governed by the applicable Creative Commons License

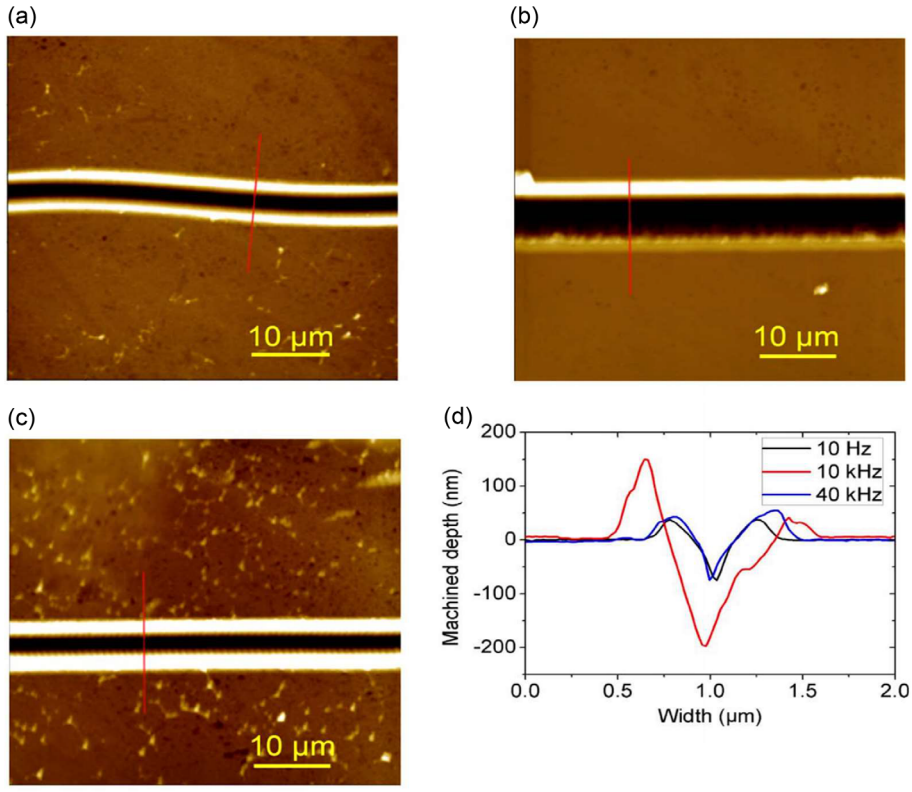

Figure 8. Micrographs of machined grooved acquired from AFM at various frequencies: a) 10 Hz, b) 10 kHz, c) 40 kHz for a stage velocity of 100 μm s^{-1} through the 'edge-forward' feed direction and d) equivalent groove cross-sections. Reproduced (Adapted) with permission.[178] Copyright 2018, Elsevier.

4.5. Energy Storage and Research

The widespread application of AFM has continued to contribute in addressing the demand for alternative energy sources and in the development of groundbreaking technology with sustainable materials for effective off-grid electricity generation. This has been actualized through the utilization of the conventional AFM technique or via the implementation of the different operational modes such the PC-AFM, KPFM, and trEFM for material characterization. The precise atomic-scale measurement of the interaction forces or electrostatic forces between the cantilever tip and the surface of a material as controlled by the piezoelectric tube, which generates sinusoidal electronic signals, has enabled AFM as an effective technique for investigating the microstructure and electrochemical processes in materials for prospective applications toward the development of energy efficient devices. For instance, the general performances of solar cells, supercapacitors, and batteries are related to both the morphology and electrochemical properties of the materials used in fabricating these devices. This implies that a comprehensive understanding of the morphological properties of a material is a crucial step toward achieving optimum efficiency and device stability. AFM is a reliable advanced imaging tool for the development and morphological characterization of new exciting materials for energy application. An advanced experimental setup for conducting photothermal measurements which incorporates AFM has been used to investigate nonradiative recombination properties of $Cu(In,Ga)Se_2$ (CIGS) solar cells.[190] The effective utilization of AFM technique can be vital in conducting innovative research in the energy sector through the characterization and predictive analytics of photovoltaic cells, modules, and devices for long-term performance optimization. Other areas in energy research that AFM can be employed for specialized roles include in the development of energy storage systems, degradation/defect analysis of photovoltaic cells, energy yield assessment, and mechanical systems such as flywheels. An important class of material which is widely investigated because of its aptitude for energy storage applications known as CNTs has been extensively characterized using AFM.[191] Nanostructure properties that can be investigated on CNTs using AFM include (although not limited to) the homogeneity, dispersibility and purity of the material. As a result of their great mechanical performance, CNTs have been reported to display extraordinary ability for the development of flywheels for kinetic energy storage with elevated energy density (8571 Wh Kg^{-1}) and increased power density (2 MW Kg^{-1}–2 GW Kg^{-1}).[192] The application of AFM can further be extended toward the investigation of interfacial features, surface heterogeneity, crystallinity, and phase changes on promising nanomaterials for the purpose of assessing their suitability in solar cell development.

4.6. Enhancement of Metabolic and Microbial Processes for Renewable Energy Applications

A lot of research activities are focused on exploration of promising materials and techniques for clean and renewable energy

© 2023 Wiley-VCH GmbH

18626319, 2024, 3, Downloaded from https://onlinelibrary.wiley.com/doi/10.1002/pssa.202300293 by University Of Fort Hare, Wiley Online Library on [02/09/2025]. See the Terms and Conditions (https://onlinelibrary.wiley.com/terms-and-conditions) on Wiley Online Library for rules of use; OA articles are governed by the applicable Creative Commons License

applications. One of such approaches which is currently trending is biogas which can be extracted by means of biodegradation process from microorganisms. Recent advances in structural biology indicate that AFM is one of the reliable techniques that can be used for functional imaging[193] and probing microbial processes.[194,195] Knowledge of metabolic and microbial processes is critical for the effective production of biogas and hence actualization of renewable energy goals.

5. Summary and Outlooks

The evolution of AFM and its various modes since inception has prompted an extension of its functionalities to perform a wide range of measurements at nanoscale. The extension of AFM capabilities has gained the attention of the research community especially in the photovoltaic sector where it has been established as a suitable technique for solar cell characterization. As a result of the broad scope of the literature and large quantities of bibliometric data contained in present work, novel ideas which stemmed from this systematic review provide the state of logical structure and emerging trends that can be useful in monitoring and evaluating the properties of solar energy-producing materials and devices. AFM application has continued to play a critical role in understanding the complexities associated with solar cell design for the purpose of improving the device performance. The summary of advances in trends deduced from this research enhances knowledge on the capabilities of AFM and its applications in solar cell characterization. It is imperative to indicate that the conclusion derived from this review is fundamental and upholds AFM and its associated technique as a suitable method toward achieving an effective and precise material selection for tailored application. The information contained in present work furnishes a favorable platform for formulating innovative concepts of optimizing and controlling the quality and uniformity of materials for industrial-scale device production with improved energy efficiency and capacitance.

Acknowledgements

This work was based on the research supported wholly/in part by the National Research Foundation of South Africa (grant number: 138532) and Govan Mbeki Research & Development Centre (GMRDC) at the University of Fort Hare.

Conflict of Interest

The authors declare no conflict of interest.

Keywords

atomic force microscopies, characterizations, polymers, quantum dots, solar cells

Received: April 14, 2023
Revised: October 2, 2023
Published online: December 3, 2023

[1] V. G. Nikitaev, A. N. Pronichev, T. K. Markov, M. N. Esaulov, *J. Phys.: Conf. Ser.* **2021**, *2058*, 012029.
[2] S. Choi, G. B. Jung, K. S. Kim, G. J. Lee, H. K. Park, *J. Nanosci. Nanotechnol.* **2014**, *1*, 71.
[3] M. Firtel, G. Henderson, I. Sokolov, *Ultramicroscopy* **2004**, *2–4*, 105.
[4] S. Vahabi, B. N. Salman, A. Javanmard, *Iran. J. Med. Sci.* **2013**, *38*, 76.
[5] L. Shere, Z. J. Zhang, J. A. Preece, *Johnson Matthey Technol. Rev.* **2018**, *62*, 438.
[6] P. Nguyen-Tri, P. Ghassemi, P. Carriere, S. Nanda, A. A. Assadi, D. D. Nguyen, *Polymers* **2020**, *12*, 1142.
[7] B. Alldritt, F. Urtev, N. Oinonen, M. Aapro, J. Kannala, P. Liljeroth, A. S. Foster, *Comput. Phys. Commun.* **2022**, *273*, 108258.
[8] G. Meyer, N. M. Amer, *Appl. Phys. Lett.* **1988**, *53*, 1045.
[9] S. Alexander, L. Hellemans, O. Marti, J. Schneir, V. Elings, P. K. Hansma, M. Longmire, J. Gurley, *J. Appl. Phys.* **1989**, *65*, 164.
[10] G. Neubauer, S. R. Cohen, G. M. McClelland, D. Horne, C. M. Mate, *Rev. Sci. Instrum.* **1990**, *61*, 2296.
[11] F. J. Giessibl, B. M. Trafas, *Rev. Sci. Instrum.* **1994**, *65*, 1923.
[12] G. Binnig, C. Quate, C. Gerber, *Phys. Rev. Lett.* **1986**, *56*.
[13] F. J. Giessibl, C. Gerber, G. Binnig, *J. Vac. Sci. Technol., B: Microelectron. Nanometer Struct. Process., Meas., Phenom.* **1991**, *9*, 984.
[14] F. Giessibl, *Appl. Phys. Lett.* **2000**, *76*, 1470.
[15] D. Rugar, H. J. Mamin, P. Guethner, *Appl. Phys. Lett.* **1989**, *55*, 2588.
[16] M. P. Murrell, M. E. Welland, S. J. O'Shea, T. M. H. Wong, J. R. Barnes, A. W. McKinnon, M. Heyns, S. Verhaverbeke, *Appl. Phys. Lett.* **1993**, *62*, 786.
[17] H. Sakaguchi, F. Iwata, A. Hirai, A. Sasaki, T. Nagamura, *Jpn. J. Appl. Phys.* **1999**, *38*, 3908.
[18] J. W. Hong, K. H. Noh, S. I. Sang-il Park, *Phys. Rev. B* **1998**, *58*, 5078.
[19] M. Nonnenmacher, M. P. O'Boyle, H. K. Wickramasinghe, *Appl. Phys. Lett.* **1991**, *58*, 2921.
[20] C. T. Gibson, G. S. Watson, S. Myhra, *Wear* **1997**, *213*, 72.
[21] O. Douheret, *High Resolution Electrical Characterization of III-V Materials and Devices*, The Royal Institute of Technology Sweden, Stockholm **2004**.
[22] R. Garcıa, R. Pérez, *Surf. Sci. Rep.* **2002**, *47*, 197.
[23] Q. Zhong, D. Inniss, K. Kjoller, V. B. Elings, *Surf. Sci.* **1993**, *290*, L688.
[24] G. Enevoldsen, *Scanning Probe Microscopy of a Metal Oxide Surface - A Detailed Study of the TiO2 (110) Surface*, Interdisciplinary Nanoscience Center (iNANO) and Department of Physics & Astronomy, University of Aarhus, Denmark, Aarhus **2007**.
[25] V. L. Mironov, *Fundamentals of Scanning Probe Microscopy*, Nizhny Novgorod: The Russian Academy of Sciences, Institute of Physics for Microstucures **2004**.
[26] S. Kremmer, H. Wurmbauer, C. Teichert, G. Tallarida, S. Spiga, C. Wiemer, M. Fanciulli, *J. Appl. Phys.* **2005**, *97*, 074315.
[27] A. Olbrich, B. Ebersberger, C. Boit, in *Proc. of the 36th Annual Int. Reliability Physics Symp.*, IEEE, Reno, NV **1998**, pp. 163–168.
[28] I. Beinik, B. Galiana, M. Kratzer, C. Teichert, I. Rey-Stolle, C. Algora, P. Tejedor, *J. Vac. Sci. Technol., B: Nanotechnol. Microelectron.: Mater., Process., Meas., Phenom.* **2010**, *28*, C5G5.
[29] P. Tejedor, L. Díez-Merino, I. Beinik, C. Teichert, *Appl. Phys. Lett.* **2009**, *95*, 123103.
[30] S. Kremmer, A. Peissl, C. Teichert, F. Kuchar, H. Hofer, *Mater. Sci. Eng., B* **2003**, *102*, 88.
[31] G. Capizzi, G. Lo Sciuto, C. Napoli, R. Shikler, M. Woźniak, *Energies* **2018**, *11*, 1.
[32] M. Moczała, N. Sosa, A. Topol, T. Gotszalk, *Ultramicroscopy* **2014**, *141*, 1.
[33] S. Sadewasser, C. Leendertz, F. Streicher, M. Ch Lux-Steiner, *Nanotechnology* **2009**, *20*, 505503.
[34] B. Moores, F. Hane, L. Eng, Z. Leonenko, *Ultramicroscopy* **2010**, *110*, 708.

© 2023 Wiley-VCH GmbH

18626319, 2024, 3, Downloaded from https://onlinelibrary.wiley.com/doi/10.1002/pssa.202300293 by University Of Fort Hare, Wiley Online Library on [02/09/2025]. See the Terms and Conditions (https://onlinelibrary.wiley.com/terms-and-conditions) on Wiley Online Library for rules of use; OA articles are governed by the applicable Creative Commons License

[35] J. Colchero, A. Gil, A. M. Baró, *Phys. Rev. B* **2001**, *64*, 245403.
[36] T. Hochwitz, A. K. Henning, C. Levey, C. Daghlian, J. Slinkman, *J. Vac. Sci. Technol., B: Microelectron. Nanometer Struct. Process., Meas., Phenom.* **1996**, *14*, 457.
[37] F. Bocquet, L. Nony, C. Loppacher, T. Glatzel, *Phys. Rev. B* **2008**, *78*, 035410.
[38] L. Nony, F. Bocquet, C. Loppacher, T. Glatzel, *Nanotechnology* **2009**, *20*, 264014.
[39] L. Groenendaal, F. Jonas, D. Freitag, H. Pielartzik, J. R. Reynolds, *Adv. Mater.* **2000**, *12*, 481.
[40] A. Alekseev, A. Efimov, J. Loos, N. Matsko, J. Syurik, *Eur. Polym. J.* **2014**, *52*, 154.
[41] I. A. Morozov, *Microsc. Res. Tech.* **2021**, *84*, 1959.
[42] Y. Yamagata, H. Benten, T. Kawanishi, M. Nakamura, *ACS Appl. Polym. Mater.* **2022**, *4*, 169.
[43] J. Y. Kim, J. H. Jung, D. E. Lee, J. Joo, *Synth. Met.* **2002**, *126*, 311.
[44] O. P. Dimitriev, D. A. Grinko, Yu. V. Noskov, N. A. Ogurtsov, A. A. Pud, *Synth. Met.* **2009**, *159*, 2237.
[45] C. S. Pathak, J. P. Singh, R. Singh, *Curr. Appl. Phys.* **2015**, *15*, 528.
[46] C. S. Pathak, S. Kumar, *Recent Developments in Atomic Force Microscopy and Raman Spectroscopy for Materials Characterization*, IntechOpen, London **2022**, pp. 1–14.
[47] C. S. Pathak, J. P. Singh, R. Singh, *Appl. Phys. Lett.* **2017**, *111*, 102107.
[48] E. Van Veldhoven, H. Van der Veer, D. Maas, P. Graat, M. A. Verheijen, Y. Galagan, R. Andriessen, *Microsc. Microanal.* **2010**, *16*, 1380.
[49] K. Kochan, D. Perez-Guaita, J. Pissang, J.-H. Jiang, A. Y. Peleg, D. McNaughton, P. Heraud, B. R. Wood, *J. R. Soc. Interfaces* **2018**, *15*.
[50] C. Prater, K. Kjoller, D. Cook, R. Shetty, G. Meyers, C. Reinhardt, J. Felts, W. King, K. Vodopyanov, A. Dazzi, *Microsc. Anal. UK* **2010**, *24*, 5.
[51] A. Dazzi, C. B. Prater, *Chem. Rev.* **2017**, *117*, 5146.
[52] J. Ye, H. Midorikawa, T. Awatani, C. Marcott, M. Lo, K. Kjoller, R. Shetty, *Microsc. Anal.* **2012**, *26*, 24.
[53] F. Tang, P. Bao, Z. Su, *Anal. Chem.* **2016**, *88*, 4926.
[54] H. L. Gao, X. W. Zhang, J. H. Meng, Z. G. Yin, L. Q. Zhang, J. L. Wu, X. Liu, *Thin Solid Films* **2015**, *576*, 81.
[55] J. S. Yun, A. Ho-Baillie, S. Huang, S. H. Woo, Y. Heo, J. Seidel, F. Huang, Y. B. Cheng, M. A. Green, *J. Phys. Chem. Lett.* **2015**, *6*, 875.
[56] J. J. Li, J. Y. Ma, Q. Q. Ge, J. S. Hu, D. Wang, L. J. Wan, *ACS. Appl. Mater. Interfaces* **2015**, *7*, 28518.
[57] Z. Zhao, X. Chen, H. Wu, X. Wu, G. Cao, *Adv. Funct. Mater.* **2016**, *26*, 3048.
[58] S. Y. Leblebici, L. Leppert, Y. Li, S. E. Reyes-Lillo, S. Wickenburg, E. Wong, J. Lee, M. Melli, D. Ziegler, D. K. Angell, D. F. Ogletree, P. D. Ashby, F. M. Toma, J. B. Neaton, I. D. Sharp, A. W. Bargioni, *Nat. Energy* **2016**, *1*, 1.
[59] Y. Kutes, Y. Zhou, J. L. Bosse, J. Steffes, N. P. Padture, B. D. Huey, *Nano Lett.* **2016**, *16*, 3434.
[60] J. Xu, A. Buin, A. H. Ip, W. Li, O. Voznyy, R. Comin, M. Yuan, S. Jeon, Z. Ning, J. J. McDowell, P. Kanjanaboos, J. P. Sun, X. Lan, L. N. Quan, D. H. Kim, I. G. Hill, P. Maksymovych, E. H. Sargent, *Nat. Commun.* **2015**, *6*, 1.
[61] A. Gomez, S. Sanchez, M. Campoy-quiles, A. Abate, *Nano Energy* **2018**, *45*, 94.
[62] J. Yang, X. Liu, Y. Zhang, X. Zheng, X. He, H. Wang, F. Yue, S. Braun, J. Chen, J. Xu, Y. Li, Y. Jin, J. Tang, C. Duan, M. Fahlman, Q. Bao, *Nano Energy* **2018**, *54*, 218.
[63] D. S. Lee, J. S. Yun, J. Kim, A. M. Soufiani, S. Chen, Y. Cho, X. Deng, J. Seidel, S. Lim, S. Huang, A. W. Y. Ho-Baillie, *ACS Energy Lett.* **2018**, *3*, 647.
[64] N. Faraji, C. Qin, T. Matsushima, C. Adachi, J. Seidel, *J. Phys. Chem. C* **2018**, *122*, 4817.
[65] C. Yang, P. Du, Z. Dai, H. Li, X. Yang, Q. Chen, *ACS Appl. Mater. Interfaces* **2019**, *11*, 14044.
[66] J. M. Howard, R. Lahoti, M. S. Leite, *Adv. Energy Mater.* **2019**, *10*, 1.
[67] W. Zhang, S. Pathak, N. Sakai, T. Stergiopoulos, P. K. Nayak, N. K. Noel, A. A. Haghighirad, V. M. Burlakov, D. W. deQuilettes, A. Sadhanala, W. Li, L. Wang, D. S. Ginger, R. H. Friend, H. J. Snaith, *Nat. Commun.* **2015**, *6*.
[68] Z. Kang, H. Si, M. Shi, C. Xu, W. Fan, S. Ma, A. Kausar, Q. Liao, Z. Zhang, Y. Zhang, *Sci. China Mater.* **2019**, *62*, 776.
[69] J. S. Yun, J. Kim, T. Young, R. J. Patterson, D. Kim, J. Seidel, S. Lim, M. A. Green, S. Huang, A. Ho-Baillie, *Adv. Funct. Mater.* **2018**, *28*, 1705363.
[70] Y. Shao, Y. Fang, T. Li, Q. Wang, Q. Dong, Y. Deng, Y. Yuan, H. Wei, M. Wang, A. Gruverman, J. E. Shield, J. Huang, *Energy Environ. Sci.* **2016**, *9*, 1752.
[71] J. Li, J.-Y. Ma, J.-S. Hu, D. Wang, L.-J. Wan, *ACS Appl. Mater. Interfaces* **2016**, *39*, 26002.
[72] B. Lee, S. Lee, D. Cho, J. Kim, T. Hwang, K. H. Kim, S. Hong, T. Moon, B. Park, *ACS Appl. Mater. Interfaces* **2016**, *45*, 30985.
[73] C. Wang, C. Xiao, Y. Yu, D. Zhao, R. A. Awni, C. R. Grice, K. Ghimire, I. Constantinou, W. Liao, A. J. Cimaroli, P. Liu, J. Chen, N. J. Podraza, C.-S. Jiang, M. M. Al-Jassim, X. Zhao, Y. Yan, *Adv. Energy Mater.* **2017**, *7*, 1700414.
[74] J. L. Garrett, E. M. Tennyson, M. Hu, J. Huang, J. N. Munday, M. S. Leite, *Nano Lett.* **2017**, *4*, 2554.
[75] S. Wieghold, J.-P. Correa-Baena, L. Nienhaus, S. Sun, K. E. Shulenberger, Z. Liu, J. S. Tresback, S. S. Shin, M. G. Bawendi, T. Buonassisi, *ACS Appl. Energy Mater.* **2018**, *1*, 6801.
[76] J. Hidalgo, A.-F. Castro-Méndez, J.-P. Correa-Baena, *Adv. Energy Mater.* **2019**, *9*, 1900444.
[77] H. Si, S. Zhang, S. Ma, Z. Xiong, A. Kausar, Q. Liao, Z. Zhang, A. Sattar, Z. Kang, Y. Zhang, *Adv. Energy Mater.* **2020**, *10*, 1903922.
[78] J. Song, Y. Zhou, N. P. Padture, B. D. Huey, *Nat. Commun.* **2020**, *11*, 1.
[79] M. Elnaggar, M. Elshobaki, A. Mumyatov, S. Y. Luchkin, N. N. Dremova, K. J. Stevenson, P. A. Troshin, *Sol. RRL* **2019**, *3*, 1.
[80] P. V. Kamat, *J. Phys. Chem. C* **2008**, *112*, 18737.
[81] V. Aroutiounian, S. Petrosyan, A. Khachatryan, K. Touryan, *J. Appl. Phys.* **2001**, *89*, 2268.
[82] L. Givaloua, M. Antoniadou, D. Perganti, M. Giannouri, C.-S. Karagianni, A. G. Kontosa, P. Falaras, *Electrochim. Acta* **2016**, *210*, 630.
[83] M. A. Basita, M. A. Abbas, H. M. Naeem, I. Ali, E. Jang, J. H. Bang, T. J. Park, *Mater. Res. Bull.* **2020**, *127*, 1.
[84] C. C. Ahia, N. Tile, Z. N. Urgessa, J. R. Botha, J. H. Neethling, *J. Cryst. Growth* **2017**, *458*, 53.
[85] C. C. Ahia, N. Tile, J. R. Botha, *J. Cryst. Growth* **2019**, *507*, 157.
[86] M. P. A. Muthalif, Y.-S. Lee, C. D. Sunesh, H.-J. Kim, Y. Choe, *Appl. Surf. Sci.* **2017**, *396*, 582.
[87] S. Sajjad, M. H. Sayyad, N. Khan, T. Manzoor, N. Nasr, R. A. Toor, S. A. A. Shah, Z. Guo, *Mater. Sci. Eng., B* **2021**, *273*, 1.
[88] M. Marandi, N. Torabi, *Opt. Mater.* **2020**, *105*, 1.
[89] H.-J. Kim, G.-C. Xu, C. V. V. M. Gopi, H. Seo, M. Venkata-Haritha, M. Shiratani, *J. Electroanal. Chem.* **2017**, *788*, 131.
[90] H.-J. Kim, L. Myung-Sik, C. V. V. M. Gopi, M. Venkata-Haritha, S. Srinivasa Rao, S.-K. Kim, *Dalton Trans.* **2015**, *44*, 11340.
[91] C. V. V. M. Gopi, M. Venkata-Haritha, H. Seo, S. Singh, S.-K. Kim, M. Shiratani, H.-J. Kim, *Dalton Trans.* **2016**, *45*, 8447.
[92] T. Archana, S. Sreelekshmi, G. Subashini, A. Nirmala Grace, M. Arivanandhan, R. Jayavel, *Int. J. Energy Res.* **2021**, *45*, 15879.
[93] P. J. Simmonds, M. Sun, R. B. Laghumavarapu, B. Liang, A. G. Norman, J.-W. Luo, D. L. Huffaker, *Nanotechnology* **2014**, *25*, 1.

© 2023 Wiley-VCH GmbH

18626319, 2024, 3, Downloaded from https://onlinelibrary.wiley.com/doi/10.1002/pssa.202300293 by University Of Fort Hare, Wiley Online Library on [02/09/2025]. See the Terms and Conditions (https://onlinelibrary.wiley.com/terms-and-conditions) on Wiley Online Library for rules of use; OA articles are governed by the applicable Creative Commons License

[94] A. G. Norman, M. C. Hanna, P. Dippo, D. H. Levi, R. C. Reedy, J. S. Ward, M. M. Al-Jassim, in *Conf. Record of the Thirty-first IEEE Photovoltaic Specialists Conf.*, US Department of Energy (US), Lake Buena Vista, FL **2005**.
[95] W.-S. Liu, H.-M. Wu, F.-H. Tsao, T.-L. Hsu, J.-I. Chyi, *Sol. Energy Mater. Sol. Cells* **2012**, *105*, 237.
[96] S. Suraprapapich, S. Thainoi, S. Kanjanachuchai, S. Panyakeow, *Sol. Energy Mater. Sol. Cells* **2006**, *90*, 2968.
[97] C. G. Bailey, D. V. Forbes, S. J. Polly, Z. S. Bittner, Y. Dai, C. Mackos, R. P. Raffaelle, S. M. Hubbard, *IEEE J. Photovoltaics* **2012**, *2*, 269.
[98] I. Ramiro, E. Antolín, M. J. Steer, P. G. Linares, E. Hernández, I. Artacho, E. López, T. Ben, J. M. Ripalda, S. I. Molina, F. Briones, C. R. Stanley, A. Martí, A. Luque, in *2012 38th IEEE Photovoltaic Specialists Conf.*, IEEE, Austin, TX **2012**.
[99] P. Kwasnicki, M. Jarzebski, P. Kardasz, M. Inglot, *Opto-Electron. Rev.* **2019**, *27*, 105.
[100] S. Maitia, F. Azlana, Y. Jadhav, J. Dana, P. Anand, S. K. Haram, G. R. Dey, H. N. Ghosh, *Sol. Energy* **2019**, *181*, 195.
[101] N. Guijarro, T. Lana-Villarreal, I. Mora-Sero, J. Bisquert, R. Gomez, *J. Phys. Chem. C* **2009**, *113*, 4208.
[102] W. Li, X. Zhong, *J. Phys. Chem. Lett.* **2015**, *6*, 796.
[103] C. V. Thulasi-Varma, S. Srinivasa Rao, C. S. S. P. Kumar, C. V. V. M. Gopi, I. K. Durga, S.-K. Kim, D. Punnoose, H.-J. Kim, *Dalton Trans.* **2015**, *44*, 19330.
[104] M. Shaheer Akhtar, J. G. Park, H. C. Lee, S. K. Lee, O. B. Yang, *Electrochim. Acta* **2010**, *55*, 2418.
[105] J. Zhang, X. Li, W. Guo, T. Hreid, J. Hou, H. Su, Z. Yuan, *Electrochim. Acta* **2011**, *56*, 3147.
[106] M. Sabet, M. Salavati-Niasari, O. Amiri, *Electrochim. Acta* **2014**, *117*, 504.
[107] S. I. Noh, H. J. Ahn, D. H. Riu, *Ceram. Int.* **2012**, *38*, 3735.
[108] J. G. Chen, H. Y. Wei, K. C. Ho, *Sol. Energy Mater. Sol. Cells* **2007**, *91*, 1472.
[109] A. de Morais, L. M. D. Loiola, J. E. Benedetti, A. S. Goncalves, C. A. O. Avellaneda, J. H. Clerici, M. A. Cotta, A. F. Nogueira, *J. Photochem. Photobiol., A* **2013**, *251*, 78.
[110] P. Gemeiner, M. Mikula, *Acta Chim. Slovaca* **2013**, *6*, 29.
[111] M. A. Sangamesha, K. Pushpalatha, G. L. Shekar, S. Shamsundar, *ISRN Nanomater.* **2013**, *2013*.
[112] M. Hossein Bazargan, M. Malekshahi Byranvand, A. N. Kharat, *Int. J. Mater. Res.* **2012**, *103*, 347.
[113] P. L. Kharel, F. P. Zamborini, B. W. Alphenaar, *J. Electrochem. Soc.* **2018**, *165*, H52.
[114] S. Prasad, G. Durai, D. Devaraj, M. S. AlSalhi, J. Theerthagiri, P. Arunachalam, M. Gurulakshmi, M. Raghavender, P. Kuppusami, *RSC Adv.* **2018**, *8*, 8828.
[115] K. T. Dembele, G. S. Selopal, R. Milan, C. Trudeau, D. Benetti, A. Soudi, M. M. Natile, G. Sberveglieri, S. Cloutier, I. Concina, F. Rosei, A. Vomiero, *J. Mater. Chem. A* **2015**, *3*, 2580.
[116] W. E. Ghann, H. Kang, J. Uddin, F. A. Chowdhury, S. I. Khondaker, M. Moniruzzaman, Md H. Kabir, M. M. Rahman, *ChemEngineering* **2019**, *3*, 1.
[117] J. T. Park, D. K. Roh, R. Patel, E. Kim, D. Y. Ryu, J. H. Kim, *J. Mater. Chem.* **2010**, *20*, 8521.
[118] J. A. He, R. Mosurkal, L. A. Samuelson, L. Li, J. Kumar, *Langmuir* **2003**, *19*, 2169.
[119] D. Paul Joseph, M. Saravanan, B. Muthuraaman, P. Renugambal, S. Sambasivam, S. Philip Raja, P. Maruthamuthu, C. Venkateswaran, *Nanotechnology* **2008**, *19*, 1.
[120] J. Guan, J. Zhang, T. Yu, G. Xue, X. Yu, Z. Tang, Y. Wei, J. Yang, Z. Li, Z. Zou, *RSC Adv.* **2012**, *2*, 7708.
[121] P. Marquet, G. Andersson, A. Snedden, L. Kloo, R. Atkin, *Langmuir* **2010**, *26*, 9612.
[122] T. Stergiopoulos, A. Ghicov, V. Likodimos, D. S. T. Soukleris, J. Kunze, P. Schmuki, P. Falaras, *Nanotechnology* **2008**, *19*, 1.
[123] A. Mohajeri, A. Omidvar, *Phys. Chem. Chem. Phys.* **2015**, *17*, 22367.
[124] T. Coffey, A. Seredinski, J. N. Poler, C. Patteson, W. H. Watts, K. Baptiste, C. Zheng, J. Cody, C. J. Collison, *Thin Solid Films* **2019**, *669*, 120.
[125] F. C. Wu, K. C. Tung, W. Y. Chou, F. C. Tang, H. L. Cheng, *Org. Electron.* **2016**, *29*, 120.
[126] T.-F. Guo, T.-C. Wen, G. L. Pakhomov, X.-G. Chin, S.-H. Liou, P.-H. Yeh, C.-H. Yang, *Thin Solid Films* **2008**, *516*, 3138.
[127] M. F. Xu, L. S. Cui, X. Z. Zhu, C. H. Gao, X. B. Shi, Z. M. Jin, Z. K. Wang, L. S. Liao, *Org. Electron.* **2013**, *14*, 657.
[128] G. L. Schulz, M. Urdanpilleta, R. Fitzner, E. Brier, E. Mena-Osteritz, E. Reinold, P. Bäuerle, *Beilstein J. Nanotechnol.* **2013**, *4*, 680.
[129] D. C. Coffey, D. S. Ginger, *Nat. Mater.* **2006**, *5*, 735.
[130] R. Giridharagopal, G. E. Rayermann, G. Shao, D. T. Moore, O. G. Reid, A. F. Tillack, D. J. Masiello, D. S. Ginger, *Nano Lett.* **2012**, *12*, 893.
[131] O. G. Reid, G. E. Rayermann, D. C. Coffey, D. S. Ginger, *J. Phys. Chem. C* **2010**, *114*, 20672.
[132] P. A. Cox, M. S. Glaz, J. S. Harrison, S. R. Peurifoy, D. C. Coffey, D. S. Ginger, *J. Phys. Chem. Lett.* **2015**, *6*, 2852.
[133] L. Krishnan Jagadamma, R. G. D. Taylor, A. L. Kanibolotsky, M. T. Sajjad, I. A. Wright, P. N. Horton, S. J. Coles, I. D. W. Samuel, P. J. Skabara, *Sustainable Energy Fuels* **2019**, *3*, 2087.
[134] S. K. Hau, Y. J. Cheng, H. L. Yip, Y. Zhang, H. Ma, A. K. Y. Jen, *ACS Appl. Mater. Interfaces* **2010**, *2*, 1892.
[135] W. Ware, et al., *Polymers* **2021**, *13*, 1.
[136] K. Zhao, Q. Wang, B. Xu, W. Zhao, X. Liu, B. Yang, M. Sun, J. Hou, *J. Mater. Chem. A* **2016**, *4*, 9511.
[137] B. Yang, S. Zhang, Y. Chen, Y. Cui, D. Liu, H. Yao, J. Zhang, Z. Wei, J. Hou, *Macromolecules* **2017**, *50*, 1453.
[138] D. Yang, B. Cao, V. Körstgens, N. Saxena, N. Li, C. Bilko, S. Grott, W. Chen, X. Jiang, J. E. Heger, S. Bernstorff, P. M. Buschbaum, *ACS Appl. Energy Mater.* **2020**, *3*, 2604.
[139] M. Guide, X. D. Dang, T. Q. Nguyen, *Adv. Mater.* **2011**, *23*, 2313.
[140] J. F. Geisz, R. M. France, K. L. Schulte, M. A. Steiner, A. G. Norman, H. L. Guthrey, M. R. Young, T. Song, T. Moriarty, *Nat. Energy* **2020**, *5*, 326.
[141] G. Timò, M. Calicchio, G. Abagnale, N. Armani, E. Achilli, M. Cornelli, F. Annoni, N. Castagnetti, M. Patrini, L. C. Andreani, L. Nasi, B. Schineller, *Sol. Energy Mater. Sol. Cells* **2021**, *224*, 1.
[142] Y. Özen, N. Akin, B. Kinaci, S. Özçelik, *Sol. Energy Mater. Sol. Cells* **2015**, *137*, 1.
[143] D. Mikulik, M. Ricci, G. Tutuncuoglu, F. Matteini, J. Vukajlovic, N. Vulic, E. Alarcon-Llado, A. F. I. Morral, *Nano Energy* **2017**, *41*, 566.
[144] N. Papež, A. Gajdoš, R. Dallaev, D. Sobola, P. Sedlák, R. Motúz, A. Nebojsa, L. Grmela, *Appl. Surf. Sci.* **2020**, *510*, 1.
[145] G. Calabrese, S. Baricordi, P. Bernardoni, S. Fin, V. Guidi, D. Vincenzi, *AIP Conf. Proc.* **2014**, *1616*, 37.
[146] B. Galiana, I. Rey-Stolle, I. Beinik, C. Algora, C. Teichert, J. M. Molina-Aldareguia, P. Tejedor, *Sol. Energy Mater. Sol. Cells* **2011**, *95*, 1949.
[147] J. Long, M. Xiao, X. Huang, Z. Xing, X. Li, P. Dai, M. Tan, Y. Wu, M. Song, S. Lu, *J. Cryst. Growth* **2019**, *513*, 38.
[148] M. Feifel, J. Ohlmann, J. Benick, M. Hermle, J. Belz, A. Beyer, K. Volz, T. Hannappel, A. W. Bett, D. Lackner, F. Dimroth, *IEEE J. Photovoltaics* **2018**, *8*, 1590.
[149] S. W. Zeng, X. M. Cai, B. P. Zhang, *IEEE J. Quantum Electron.* **2010**, *46*, 783.
[150] F. Dimroth, M. Grave, P. Beutel, U. Fiedeler, C. Karcher, T. N. D. Tibbits, E. Oliva, G. Siefer, M. Schachtner, A. Wekkeli, A. W. Bett, R. Krause, M. Piccin, N. Blanc, C. Drazek, E. Guiot,

© 2023 Wiley-VCH GmbH

18626319, 2024, 3, Downloaded from https://onlinelibrary.wiley.com/doi/10.1002/pssa.202300293 by University Of Fort Hare, Wiley Online Library on [02/09/2025]. See the Terms and Conditions (https://onlinelibrary.wiley.com/terms-and-conditions) on Wiley Online Library for rules of use; OA articles are governed by the applicable Creative Commons License

B. Ghyselen, T. Salvetat, A. Tauzin, T. Signamarcheix, A. Dobrich, T. Hannappel, K. Schwarzburg, *Prog. Photovoltaics* **2014**, *22*, 277.
[151] S. Sharma, C. A. Favela, S. Sun, V. Selvamanickam, in *2020 47th IEEE Photovoltaic Specialists Conf. (PVSC)*, IEEE, Calgary, AB **2020**.
[152] P. Narchi, J. Alvarez, P. Chrétien, G. Picardi, R. Cariou, M. Foldyna, *Nanoscale Res. Lett.* **2016**, *11*, 1.
[153] A. Kikukawa, S. Hosaka, R. Imura, *Appl. Phys. Lett.* **1995**, *66*, 3510.
[154] A. Fejfar, B. Rezek, P. Knapek, J. Stuchlik, J. Kocka, *J. Non-Cryst. Solids* **2000**, *266–269*, 309.
[155] J. Heo, S. Won, *Thin Solid Films* **2013**, *546*, 353.
[156] A. Fashina, K. K. Adama, L. A. Abdullah, C. J. Ani, O. K. Oyewole, J. Asare, V. C. Anye, *Int. J. Phys. Res.* **2018**, *6*, 13.
[157] L. Borowik, H. Lepage, N. Chevalier, D. Mariolle, O. Renault, *Nanotechnology* **2014**, *25*, 1.
[158] C. C. Ahia, N. Tile, E. L. Meyer, J. R. Botha, *Mater. Sci. Semicond. Process.* **2021**, *127*, 1.
[159] J. S. Hwang, M. C. Kao, J. M. Shiu, C. N. Fan, S. C. Ye, W. S. Yu, H. M. Lin, T. Y. Lin, S. Chattopadhyay, L. C. Chen, K. H. Chen, *J. Phys. Chem. C* **2011**, *115*, 21981.
[160] J. P. Kleider, J. Alvarez, A. V. Ankudinov, A. S. Gudovskikh, E. V. Gushchina, M. Labrune, O. A. Maslova, W. Favre, M.-E. Gueunier-Farret, P. Roca I Cabarrocas, E. I. Terukov, *Nanoscale Res. Lett.* **2011**, *6*, 152.
[161] O. A. Maslova, J. Alvarez, E. V. Gushina, W. Favre, M. E. Gueunier-Farret, A. S. Gudovskikh, A. V. Ankudinov, E. I. Terukov, J. P. Kleider, *Appl. Phys. Lett.* **2010**, *97*, 252110.
[162] B. Rezek, T. Mates, E. Sipek, J. Stuchlik, A. Fejfar, J. Kocka, *J. Non-Cryst. Solids* **2002**, *299–302*, 360.
[163] M. J. Romero, F. Liu, O. Kunz, J. Wong, C.-S. Jiang, M. M. Al-Jassim, A. G. Aberle, *Mater. Res. Soc. Symp. Proc.* **2009**, *1153*.
[164] R. S. Dubey, D. K. Gautam, *J. Optoelectron. Biomed. Mater.* **2009**, *1*, 8.
[165] J. P. Kleider, C. Longeaud, R. Bruggemann, F. Houze, *Thin Solid Films* **2001**, *383*, 57.
[166] I. Simkiene, V. Snitka, K. Naudzius, V. Pacebutas, M. Rackaitis, in *Part of the Symp. on Design. Test, and Microfabrication of MEMS and MOEMS*, SPIE Digital Library, Paris, France **1999**.
[167] P. Willke, W. Paul, F. D. Natterer, K. Yang, Y. Bae, T. Choi, J. Fernández-Rossier, A. J. Heinrich, C. P. Lutz, *Sci. Adv.* **2018**, *4*, 1.
[168] G. Binnig, H. Rohrer, C. Gerber, E. Weibel, *Phys. Rev. Lett.* **1983**, *50*, 120.
[169] O. M. Gordon, P. J. Moriarty, *Mach. Learn.: Sci. Technol.* **2020**, *1*, 023001.
[170] Y. Kobayashi, Y. Miyake, F. Ishiwari, S. Ishiwata, A. Saeki, *RSC Adv.* **2023**, *13*, 15107.
[171] T. Sun, Y. D. Yan, J. F. Xia, S. Dong, Y. C. Liang, K. Cheng, *Key Eng. Mater.* **2004**, *259–260*, 577.
[172] Z. J. Hu, S. G. Zhang, X. H. Zheng, Y. D. Yan, T. Sun, Q. L. Zhao, S. Dong, *Key Eng. Mater.* **2006**, *315–316*, 800.
[173] H. Zhou, J. Deng, *Procedia Manuf.* **2020**, *48*, 508.
[174] S. Miyake, *Appl. Phys. Lett.*, **1995**, *67*, 2925.
[175] H. J. Mamin, D. Rugar, *Appl. Phys. Lett.*, **1992**, *61*, 1003.
[176] H. T. Lee, J. S. Oh, S. J. Park, K. H. Park, J. S. Ha, H. J. Yoo, J. Y. Koo, *J. Vac. Sci. Technol., A* **1997**, *15*, 1451.
[177] S. Miyake, M. Wang, J. Kim, *J. Nanotechnol.* **2014**, *2014*, 1.
[178] Y. Geng, E. B. Brousseau, X. Zhao, M. Gensheimer, C. R. Bowen, *Precis. Eng.* **2018**, *51*, 536.
[179] D. Wang, L. Tsau, K. L. Wang, *Appl. Phys. Lett.* **1994**, *65*, 1415.
[180] R. D. Piner, J. Zhu, F. Xu, S. Hong, C. A. Mirkin, *Science* **1999**, *283*, 661.
[181] L. L. Sohn, R. L. Willett, *Appl. Phys. Lett.* **1995**, *67*, 1552.
[182] H. Bai, S. Wu, *Nanotechnol. Precis. Eng.* **2021**, *4*, 1.
[183] K. C. Chang, Y. W. Chiang, C. H. Yang, J. W. Liou, *Tzu Chi Med. J.* **2012**, *24*, 162.
[184] E. Miller, T. Garcia, S. Hultgren, A. F. Oberhauser, *Biophys. J.* **2006**, *91*, 3848.
[185] C. McAllister, M. A. Kartmov, Y. Kawano, A. Y. Lushnikov, A. Mikheikin, V. N. Uversky, Y. L. Lyubchenko, *J. Mol. Biol* **2005**, *354*, 1028.
[186] Y. G. Kuznetsov, C. Xiao, S. Sun, D. Raoult, M. Rossmann, A. McPherson, *Virology* **2010**, *404*, 127.
[187] Y. Kuznetsov, P. D. Gershon, A. McPherson, *J. Virol.* **2008**, *82*, 7551.
[188] O. Hoshi, T. Ushiki, in *Atomic Force Microscopy In Biomedical Research. Methods In Molecular Biology*, Humana Press, Totowa, NJ **2011**, pp. 109–115.
[189] T. Ushiki, M. Shigeno, O. Hoshi, *Nanotechnology* **2008**, *19*, 384022.
[190] Y. Hamamoto, K. Hara, T. Minemoto, T. Takahashi, *Sol. Energy Mater. Sol. Cells* **2015**, *141*, 32.
[191] S. Bellucci, G. Gaggiotti, M. Marchetti, F. Micciulla, R. Mucciato, M. Regi, *J. Phys.: Conf. Ser.* **2007**, *61*, 99.
[192] Y. Bai, B. Shen, S. Zhang, Z. Zhu, S. Sun, J. Gao, B. Li, Y. Wang, R. Zhang, F. Wei, *Adv. Mater.* **2018**, *31*.
[193] A. C. Dumitru, M. Koehler, *J. Struct. Biol.* **2023**, *215*, 107963.
[194] M. Li, *Atomic Force Microscopy for Nanoscale Biophysics*, Academic Press, Amsterdam, Netherlands **2023**, pp. 187–217.
[195] S. Kandapal, B. Xu, *Processes* **2023**, *11*, 2430.
[196] X. Fan, W. Nie, H. Tsai, N. Wang, H. Huang, Y. Cheng, R. Wen, L. Ma, F. Yan, Y. Xia, *Adv. Sci.* **2019**, *6*, 1.
[197] M. Palewicz, A. Sikora, T. Piasecki, E. Gacka, P. Nitschke, P. Gnida, B. Jarząbek, T. Gotszalk, *Energies* **2023**, *16*, 4741.
[198] H. Sha, J. Han, F. Wang, W. Huang, X. Ma, C. Jia, Y. Chen, *Opt. Mater.* **2023**, *139*, 113817.
[199] T. Leonhard, H. Rohm, F. J. Altermann, M. J. Hoffmann, A. Colsmann, *J. Mater. Chem. A* **2021**, *9*, 21845.
[200] L. Xiao, X. Xu, Z. Lu, J. Zhao, R. Liu, Y. Ye, R. Tang, W.-Q. Liao, R.-G. Xiong, G. Zou, *Nano Energy* **2023**, *107*, 108114.
[201] M. Esteves, D. Mombrú, M. Romero, L. Fernández-Werner, R. Faccio, A. W. Mombrú, *Mater. Today Electron.* **2023**, *3*, 100029.
[202] M. K. A. A. Al-Byati, A. M. J. Al-Duhaidahawi, *Biomed. Chem. Sci.* **2023**, *2*, 48.
[203] B. Y. Kadem, Z. Y. Abbas, R. K. Husein, T. F. Najm, *AIP Conf. Proc.* **2023**, *2769*.

Chinedu C. Ahia is a research fellow in photonics and materials characterization at the Fort Hare Institute of Technology, University of Fort Hare where he spearheads the operations and training on confocal Raman/atomic force microscope. He was conferred a Ph.D. in physics by Nelson Mandela University in 2018. His expertise includes growth, characterization and development of semiconductor materials, quantum dots, quantum wells, superlattices, and smart nanomaterials for optoelectronic device applications. He is a professional member of the South African Institute of Physics (SAIP) among many others and the author of several articles in reputable/accredited journals and book chapters.

© 2023 Wiley-VCH GmbH

18626319, 2024, 3, Downloaded from https://onlinelibrary.wiley.com/doi/10.1002/pssa.202300293 by University Of Fort Hare, Wiley Online Library on [02/09/2025]. See the Terms and Conditions (https://onlinelibrary.wiley.com/terms-and-conditions) on Wiley Online Library for rules of use; OA articles are governed by the applicable Creative Commons License

Edson Meyer obtained his Ph.D. in physics from the University of Port Elizabeth in 2002. He is currently a full professor at the University of Fort Hare and the Director of the Fort Hare Institute of Technology. Professor Meyer has served as Head of the Department of Physics at the University of Fort Hare and as nonexecutive director on the boards of the South African National Energy Development Institute (SANEDI) and the Digitisation and Refurbishment Institute of South Africa (DRISA). He has published over 142 peer-reviewed articles, with over 5900 citations, an h-index of 34, and i10-index of 82.

© 2023 Wiley-VCH GmbH

18626319, 2024, 3, Downloaded from https://onlinelibrary.wiley.com/doi/10.1002/pssa.202300293 by University Of Fort Hare, Wiley Online Library on [02/09/2025]. See the Terms and Conditions (https://onlinelibrary.wiley.com/terms-and-conditions) on Wiley Online Library for rules of use; OA articles are governed by the applicable Creative Commons License